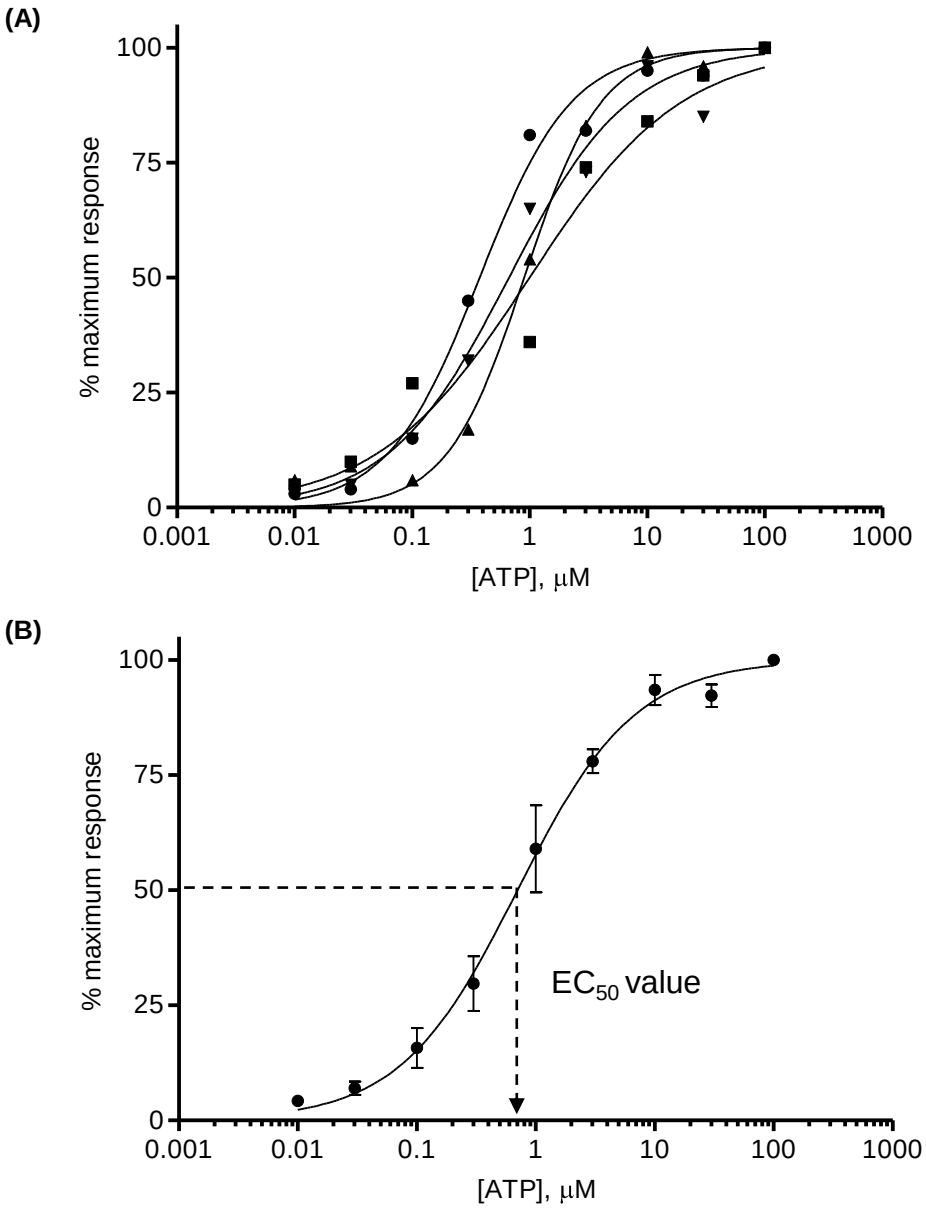

Figure 3.2. ATP sensitivity at the human P2X1 receptor.
Agonist action was tested on oocytes expressing the WT P2X1 receptor by two-electrode voltage clamp electrophysiology (holding potential -60mV). **(A)** Individual concentration-response curves to ATP at the WT P2X1 receptor. **(B)** Average of the concentration-response curves to ATP at the WT P2X1 receptor. The EC_{50} value is shown by the dashed line. Error bars indicate S.E.M.

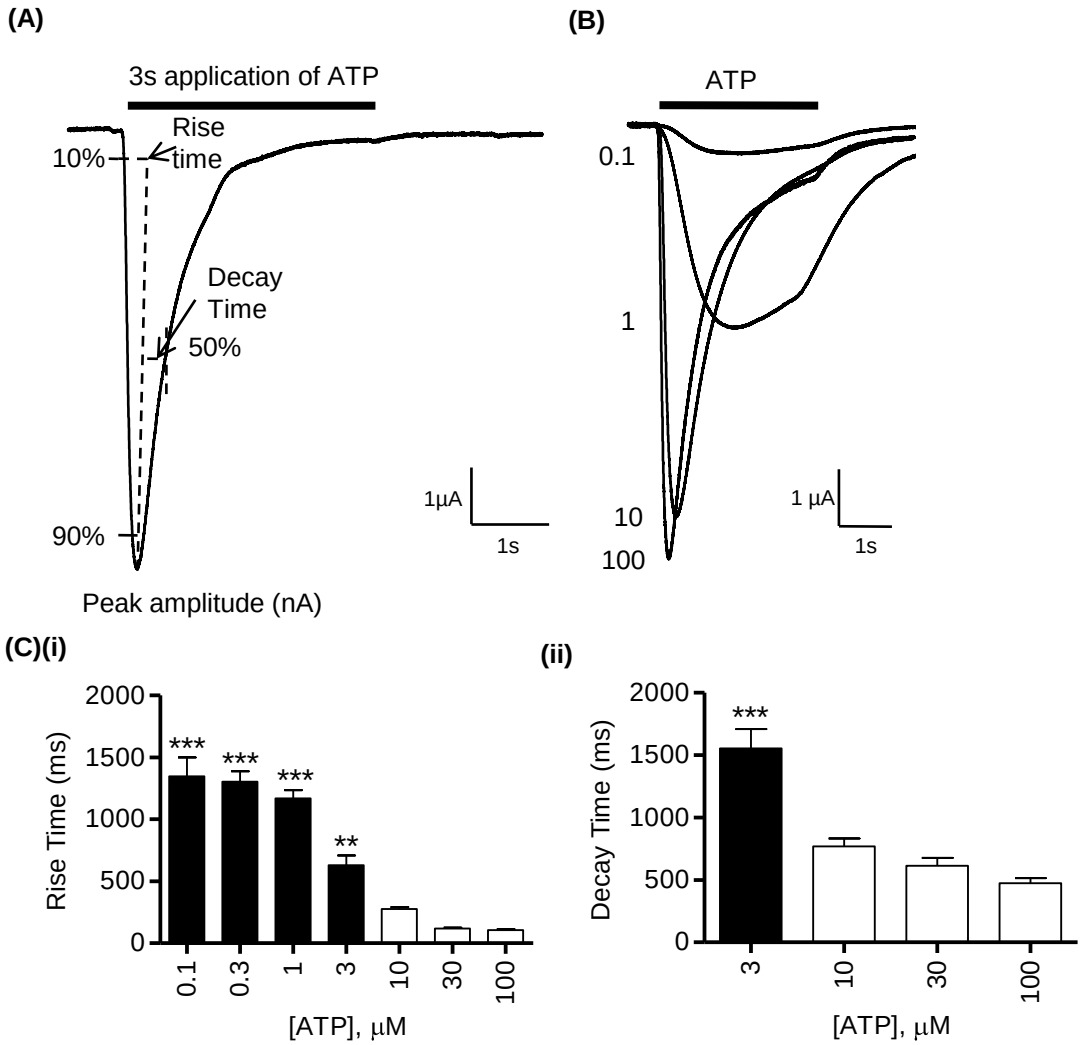

Figure 3.3. ATP-evoked currents at the human P2X1 receptor.
(A) ATP-evoked current at the P2X1 receptor to 100 µM ATP. The dotted lines represent the position where the rise-times (10 to 90%) and decay-times (100 to 50%) were calculated. **(B)** ATP-evoked inward currents in the presence of different concentrations of ATP at the WT P2X1 receptor. Black bar represents 3 second application of ATP, concentration of ATP is in µM. **(C)** The time-course of the individual concentrations of ATP showing the **(i)** rise-times and **(ii)** decay-times. The decay-time could not be calculated at concentrations of ATP lower than 3 µM as the response did not decay below 50% of the peak current amplitude during the 3s application of ATP. Significant differences from the rise and decay time of the current produced with 100 µM ATP are indicated in black *(**p < 0.01, *** p < 0.001*, n = 5 to 10). Error bars indicate S.E.M.

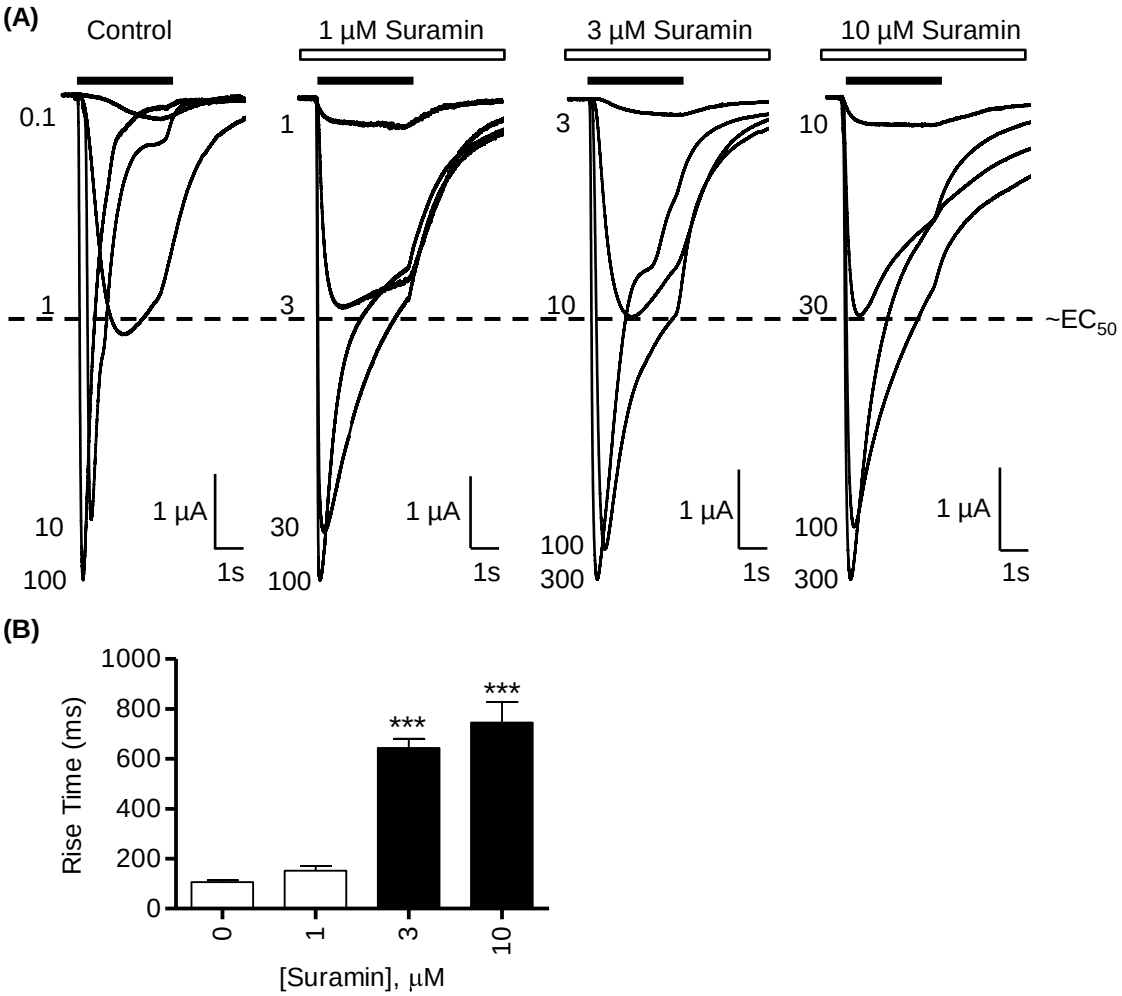

Figure 3.4. Antagonism of WT P2X1 receptor currents by suramin.
(A) ATP-evoked inward currents produced at the WT P2X1 receptor in the absence (control) and the presence of 1, 3 and 10 µM suramin. Black bar indicates 3 second co-application of ATP and suramin, open bar indicates the application of suramin throughout the recording, concentrations in µM. Dotted line represents the ~EC_{50} concentration of ATP. **(B)** The rise-time (10% to 90%) of 10 µM ATP in the absence and presence of different concentrations of suramin. Significant differences from the rise time of the current produced in the absence of suramin are indicated in black (*** $p < 0.001$, n = 3 to 5). Error bars indicate S.E.M.

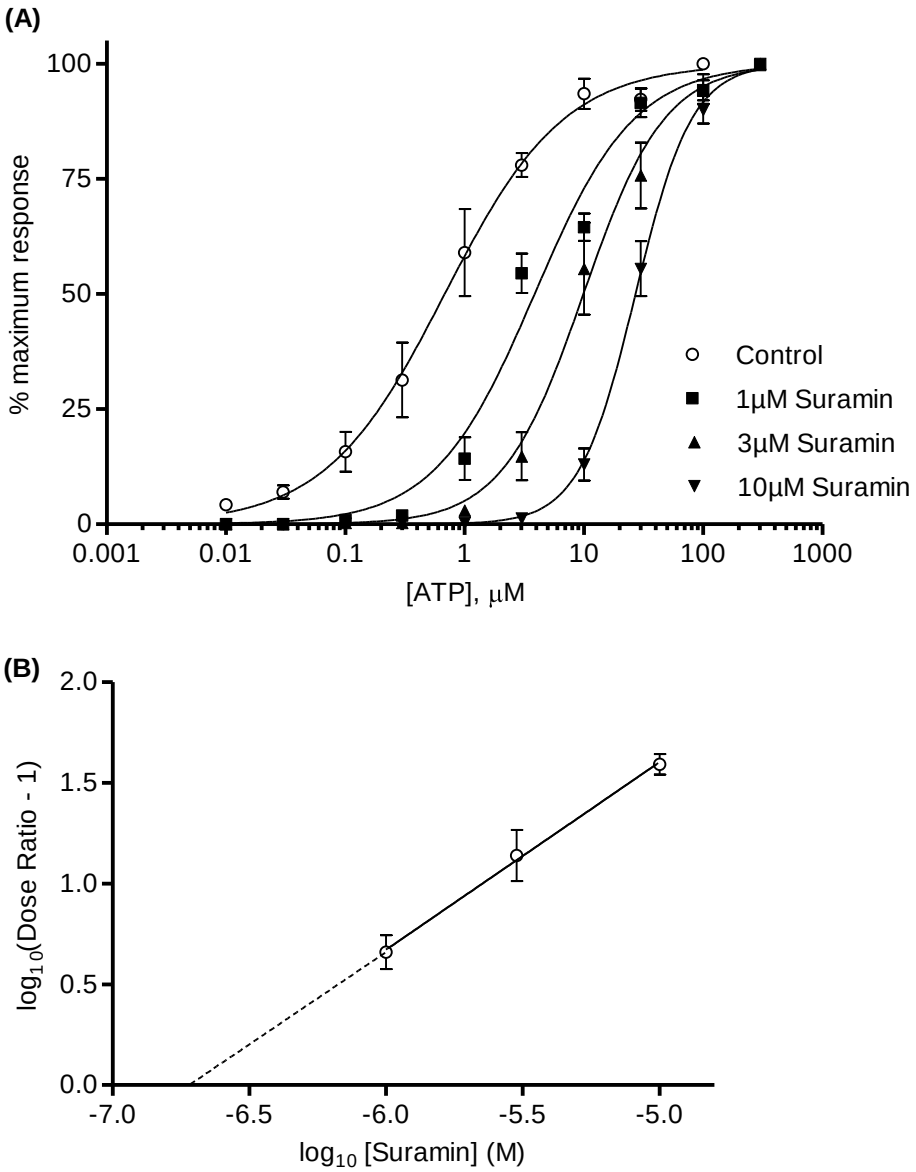

Figure 3.5. Concentration-dependent antagonism of the WT P2X1 receptor by suramin. **(A)** Concentration-response curves of the WT P2X1 receptor with ATP in the presence of different concentrations of suramin (1, 3 and 10 μM). **(B)** Schild plot analysis of suramin action at the P2X1 receptor. n = 3 to 4 for all data sets. Error bars indicate S.E.M.

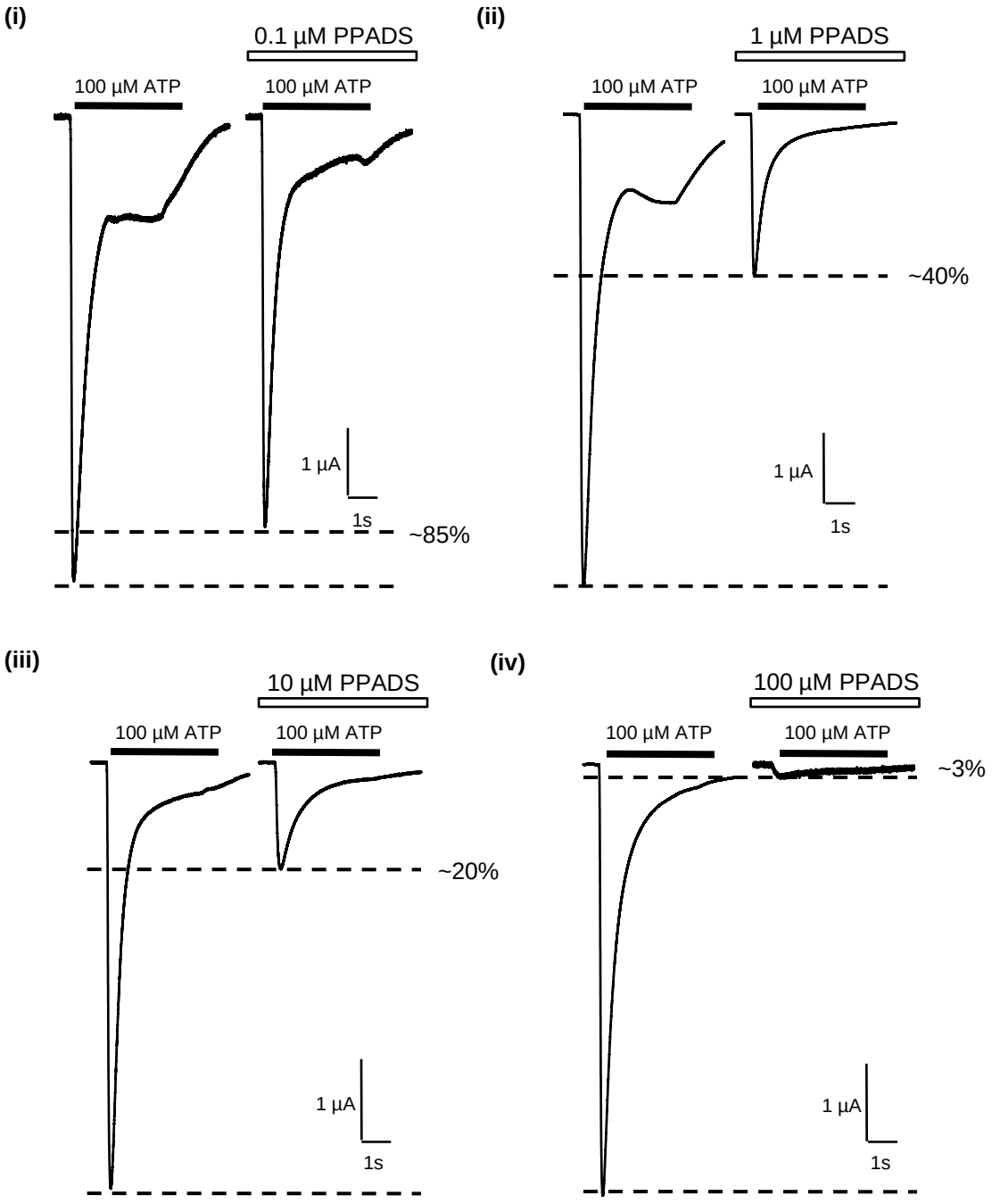

Figure 3.6. Antagonism of WT P2X1 receptor currents by PPADS.
ATP-evoked inward currents (to 100 µM ATP) produced at the WT P2X1 receptor in the absence and presence of **(i)** 0.1, **(ii)** 1, **(iii)** 10 and **(iv)** 100 µM PPADS. Black bar indicates 3 second co-application of ATP and PPADS, open bar indicates the application of PPADS throughout the recording, concentrations in µM. Approximate percentage change of the control response is shown by the dotted line.

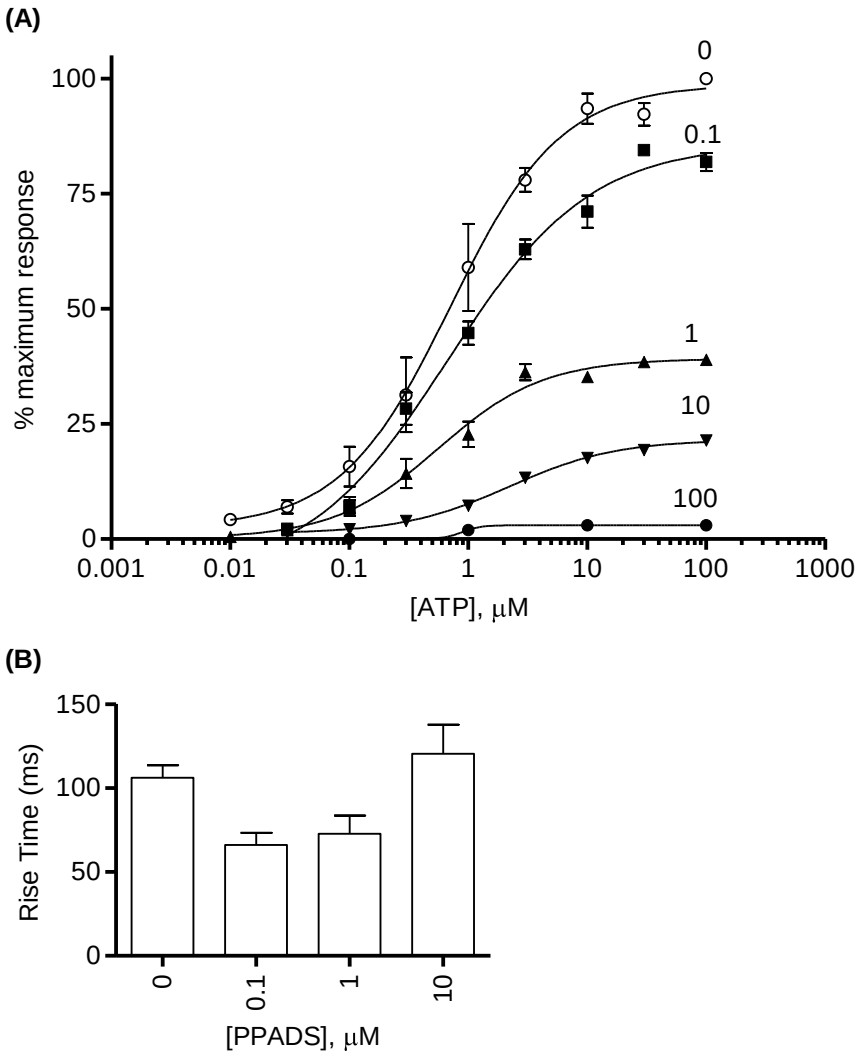

Figure 3.7. Concentration-dependent antagonism of the WT P2X1 receptor by PPADS. **(A)** Concentration-dependent responses to ATP in the presence of PPADS (0.1, 1, 10 and 100 μM). n = 3 to 4 for all data sets. **(B)** The rise-time (10% to 90% of the current amplitude) of 10 μM ATP in the absence and presence of different concentrations of PPADS. Error bars indicate S.E.M.

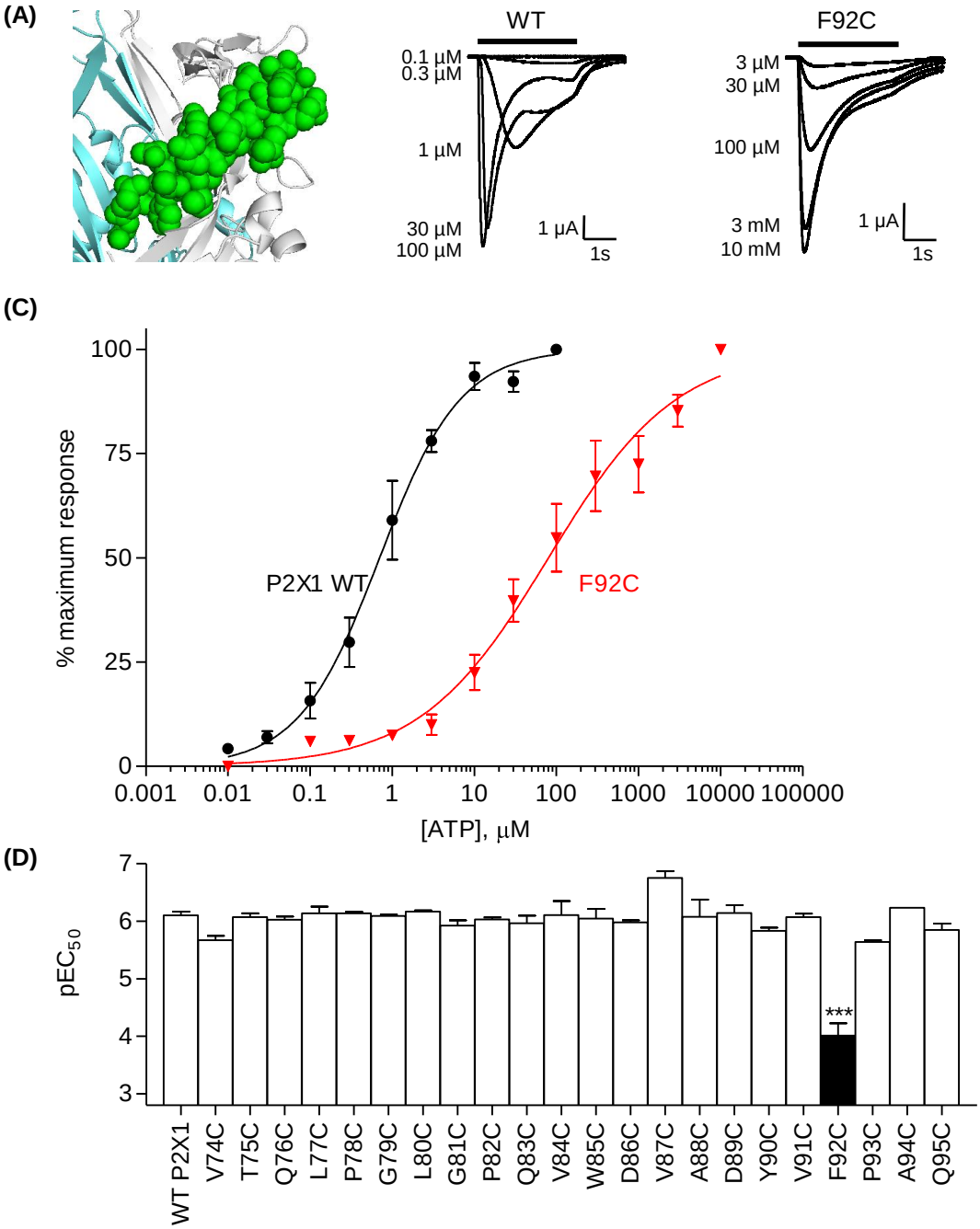

Figure 4.2 Effect on ATP potency at the P2X1 receptor mutants V74C-G96C.
(A) Residues V74 to G96 mapped onto the homology model of the P2X1 receptor, showing the residues in green spheres and two subunits in white and cyan as "cartoon" format. **(B)** Concentration responses to ATP of the WT P2X1 receptor and mutant F92C with the black bar representing 3 second application of ATP. **(B)** Concentration response curves for WT P2X1 and F92C mutant. **(C)** Summary showing pEC_{50} values of all mutants compared to WT P2X1 (left). Values are shown as means S.E.M. Significant differences from the wild type are indicated in black (***$p < 0.001$). G96C data is not shown as it has previously been characterised by Digby et al. (2005) with ATP having a pEC_{50} value of 5.27 0.07.

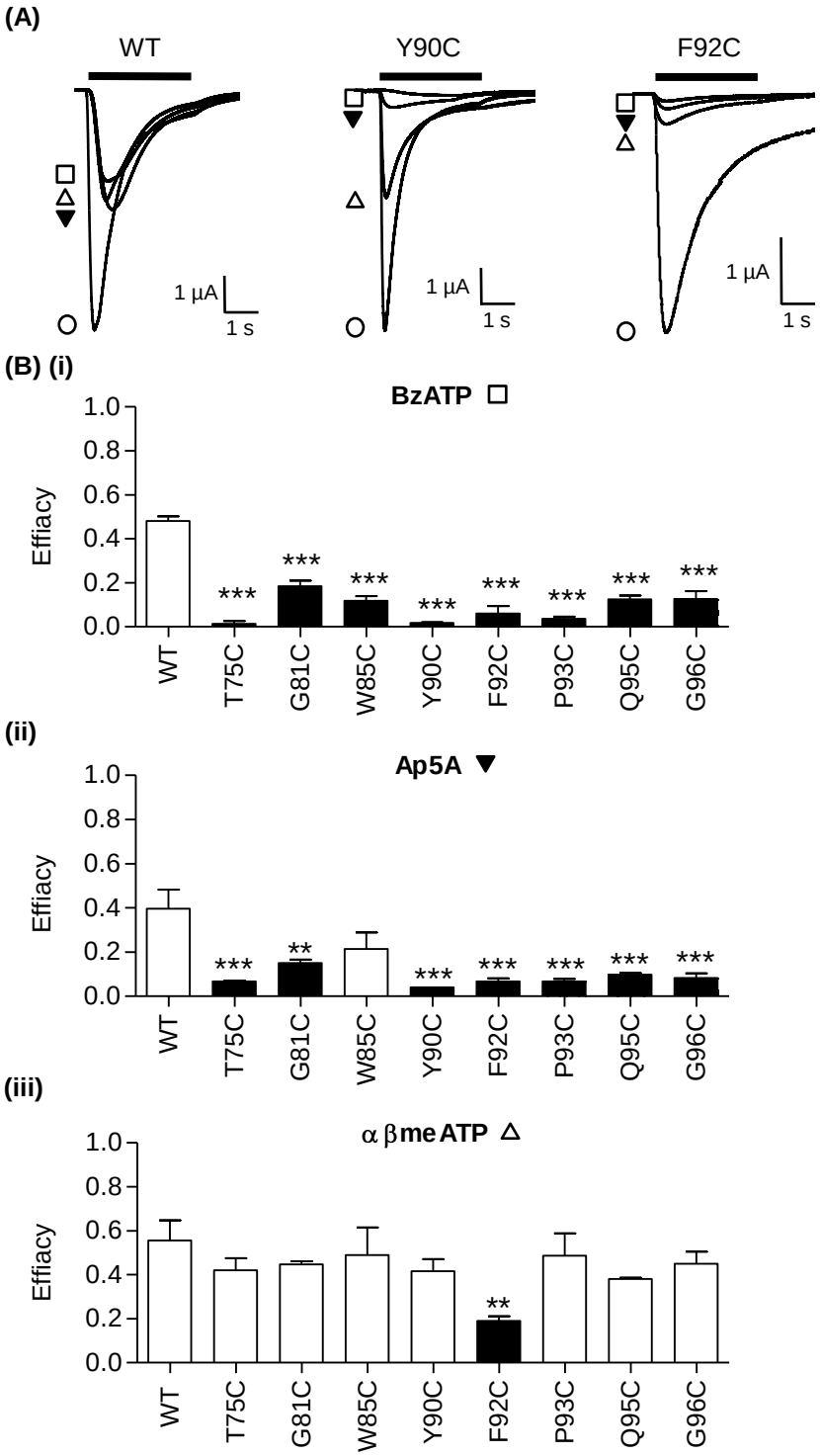

Figure 4.3 Effect on partial agonist efficacy at the P2X1 receptor mutants V74C-G96C.
(A) Representative recordings of currents evoked by partial agonists (100 µM) BzATP (open square), Ap5A (filled triangle) and α,β-meATP compared to control ATP (100 µM) (open circles) for WT and mutants Y90C and F92C. **(B)** Summary of mutants V74C-G96C demonstrating significant changes in efficacy of **(i)** BzATP and to the corresponding mutants with **(ii)** AP5A and **(iii)** α,β-meATP. Significant reductions in efficacy are shown as black bars, $^{**}p < 0.01$, $^{***}p < 0.001$ (n = 3 to 5), error bars indicate S.E.M.

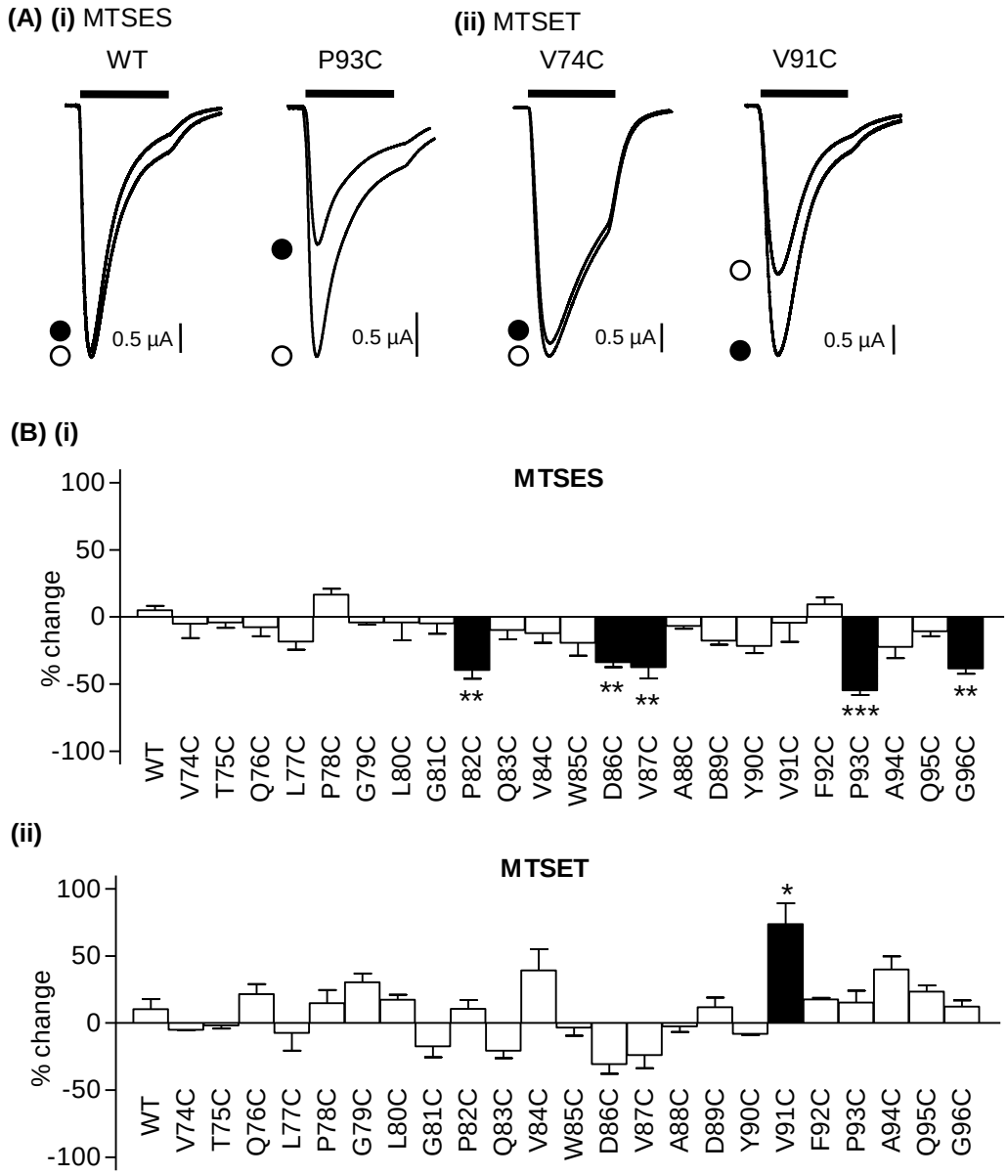

Figure 4.4. Effect of MTS reagents at P2X1 receptor mutants V74C-G96C.
(A) Effect of **(i)** MTSES and **(ii)** MTSET (both 1 mM) on an EC_{50} concentration of ATP at the P2X1 receptor mutants V74C-G96C. Open circles represent the control response in the absence of any MTS reagents and the closed circles represent the response in the presence of the MTS reagents. Black bar indicates 3 second application of ATP. (**B)** The response of mutants V74C-G96C to an EC_{50} concentration of ATP in the presence of **(i)** MTSES and **(ii)** MTSET (both 1 mM). *p < 0.05; **p < 0.01; ***p < 0.001. Error bars indicate S.E.M.

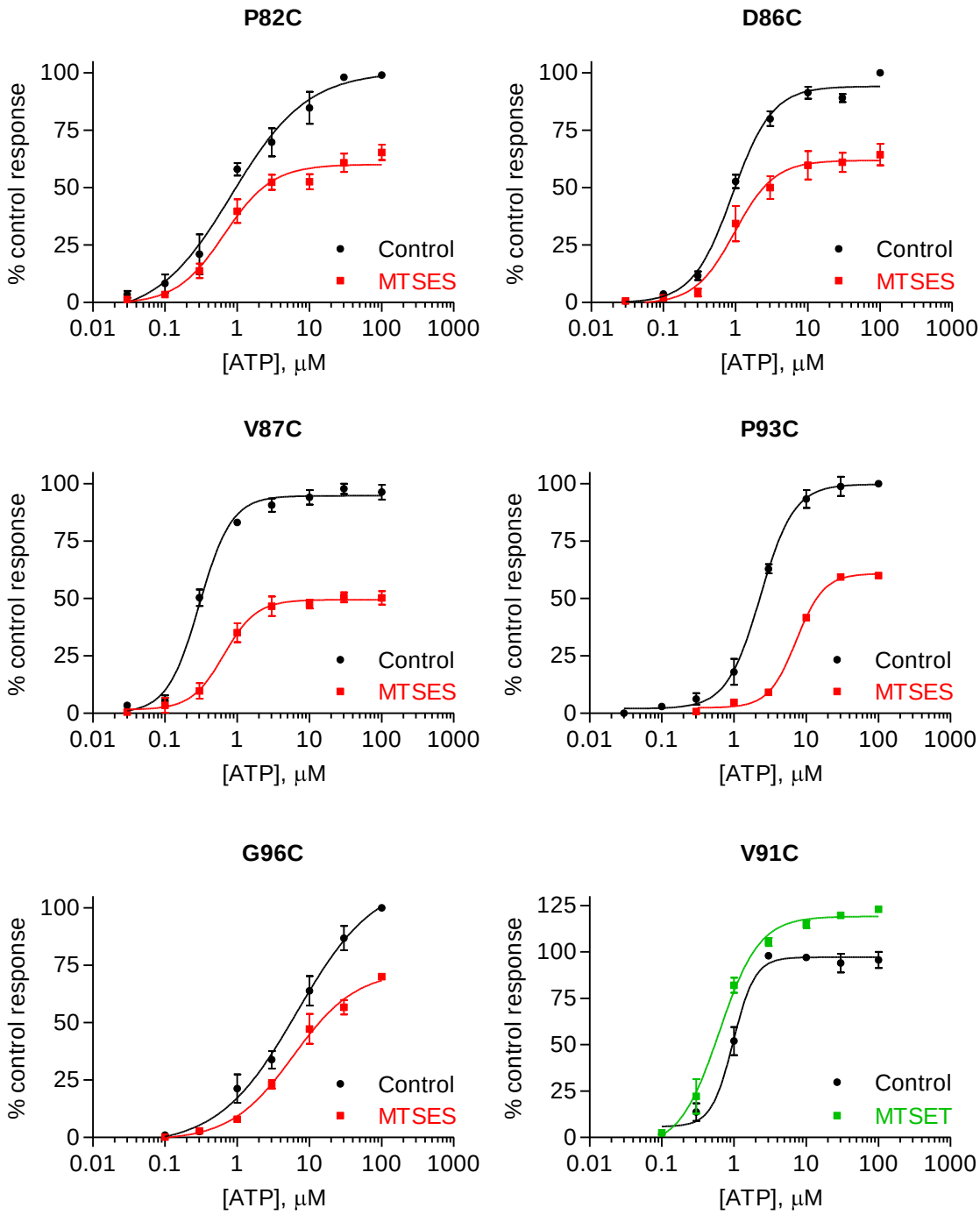

Figure 4.5. Effect of MTS reagents on the ATP potency at the P2X1 receptor mutants. Concentration-response curves of the P2X1 receptor mutants P82C, D86C, V87C, P93C and G96C with (red) and without (black) 1 mM of MTSES and V91C with (green) and without (black) 1 mM of MTSET. Mutants were incubated in the presence of the MTS reagents for 3 hours. Error bars indicate S.E.M.

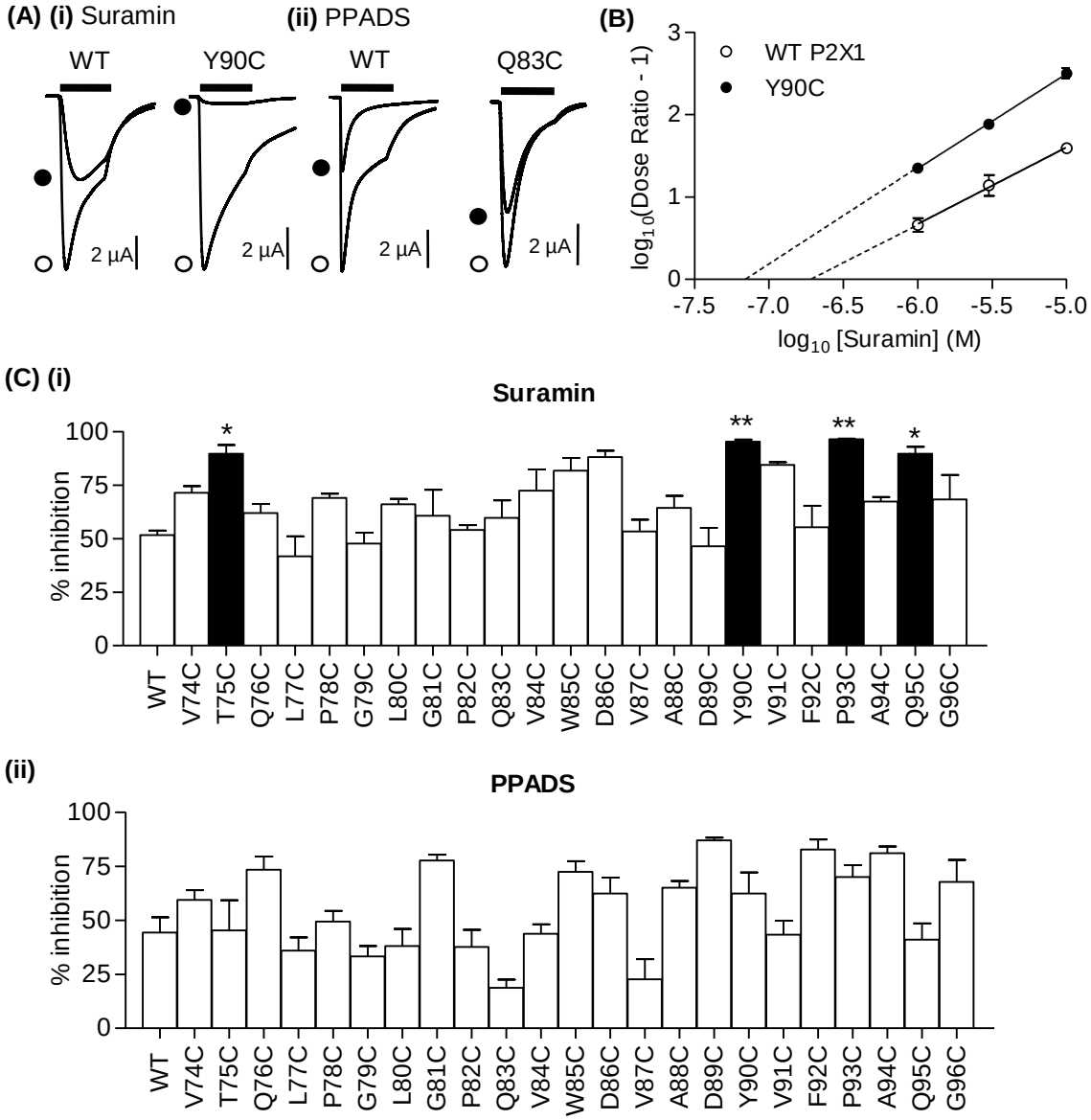

Figure 4.6. Antagonist action at P2X1 receptor mutants V74C-G96C.
Antagonists were applied to the P2X1 receptor mutants using concentrations that inhibited the EC_{90} concentration of ATP response by ~ 50% at the WT P2X1, Suramin (3 µM) and PPADS (1 µM). **(A)** Representative recordings of **(i)** Y90C, a P2X1 mutant with increased suramin sensitivity and **(ii)** Q83C, a P2X1 mutant with slightly decreased PPADS sensitivity. Traces show the response in the presence of ATP only (open circle) and in the presence of ATP and the antagonist (closed circle). ATP was applied for 3 seconds (black bar) and the antagonists were bath perfused 5 minutes before recording. **(B)** Schild plot analysis of suramin antagonism at the WT P2X1 receptor and the mutant Y90C. **(C)** % inhibition of EC_{90} concentration of ATP in the presence of the antagonists **(i)** Suramin (3 µM) and **(ii)** PPADS (1 µM) on P2X1 receptor mutants V74C-G96C (n = 3-4). *p < 0.05; **p < 0.01. Error bars indicate S.E.M.

(A)

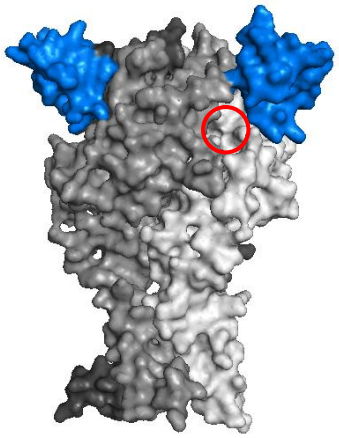

(B)

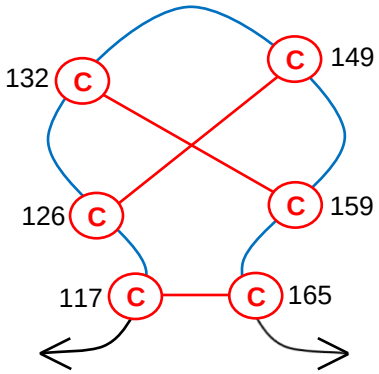

(C)

```
P2X1  1    MARRFQEELA AFLFEYDTPR MVLVRNKKVG VIFRLIQLVV LVYVIGWVFL YEKGYQT-SS
P2X2  1    MVRRLARGCW SALWDYETPK VIVVRNRRLG VLYRAVQLLI LLYFVWYVFI VQKSYQESET

P2X1 60    GLISSVSVKL KGLAVTQLPG LGPQVWDVAD YVFPAQGDNS FVVMTNFIVT PKQTQGYCAE
P2X2 61    GPESSIITKV KGITTS---- -EHKVWDVEE YVKPPEGGSV FSIITRVEAT HSQTQGTCPE

P2X1 120   HPE--GGICK EDSGCTPGKA KRKAQGIRTG KCVA-FNDTV KTCEIFGWCP VEVDDDIPRP
P2X2 116   SIRVHNATCL SDADCVAGEL DMLGNGLRTG RCVPYYQGPS KTCEVFGWCP VEDGA-SVSQ

P2X1 177   ALLREAENFT LFIKNSISFP RFKVNRRNLV EEVNAAHMKT CLFHKTLHPL CPVFQLGYVV
P2X2 175   FLGTMAPNFT ILIKNSIHYP KFHFSKGNIA DRTDG-YLKR CTFHEASDLY CPIFKLGFIV

P2X1 237   QESGQNFSTL AEKGGVVGIT IDWHCDLDWH VRHCRPIYEF HGLYE--EKN LSPGFNFRFA
P2X2 234   EKAGESFTEL AHKGGVIGVI INWDCDLDLP ASECNPKYSF RRLD-PKHVP ASSGYNFRFA

P2X1 295   RHFVE-NGTN YRHLFKVFGI RFDILVDGKA GKFDIIPTMT TIGSGIGIFG VATVLCDLLL
P2X2 293   KYYKIN-GTT TRTLIKAYGI RIDVIVHGQA GKFSLIPTII NLATALTSVG VGSFLCDWIL

P2X1 354   LHILPKRHYY KQKKFKYAED MGPGAAERDL AATSSTLGLQ ENMRTS-
P2X2 352   LTFMNKNKVY SHKKFDKVCT PSHPSGSWPV TLARVLGQAP PEPGHRSEDQ HPSPPSGQEG


P2X2 412   QQGAECGPAF PPLRPCPISA PSEQMVDTPA SEPAQASTPT DPKGLAQL-
```

Figure 5.2. Location of the cysteine rich head region on the P2X1 receptor.
(A) Surface rendered homology model of the P2X1 receptor, which is based on the crystal structure of the zP2X4 receptor. The 3 different subunits are in different shades of grey with the cysteine rich head region of each subunit in blue. The red ring highlights the location of the proposed ATP binding site in-between two subunits. **(B)** Cartoon of the pairing of cysteine disulphide bonds in the head region. **(C)** Sequence alignment of the human P2X1 and the human P2X2 receptor. The residues that were swapped in the P2X1 Cys2(1-6) chimera are shown in red.

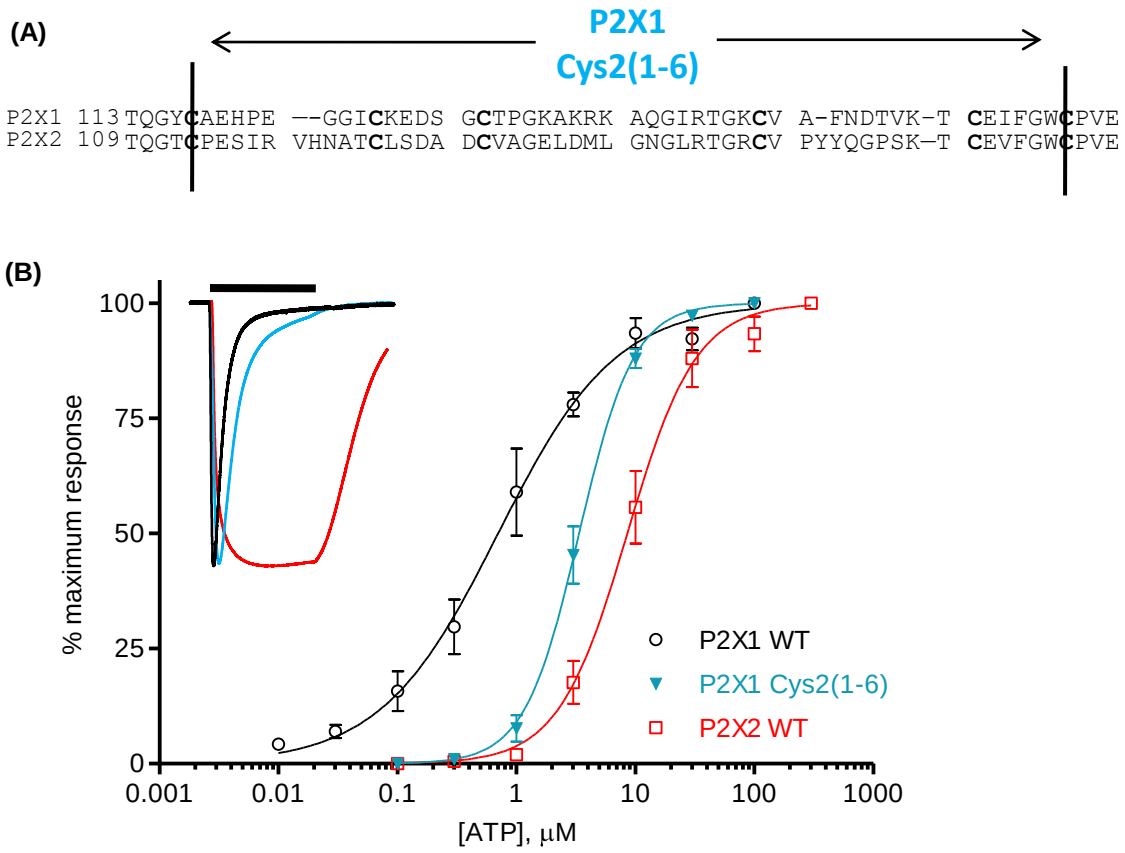

Figure 5.3. ATP potency at the P2X1 receptor, P2X2 receptor and the P2X1 Cys2(1-6) chimera.
(A) Sequence alignment of the P2X1 and the P2X2 receptors with the residues being swapped in the P2X1 Cys2(1-6) chimera shown between the black lines. Conserved cysteine residues are in bold **(B)** Concentration-response curves of the WT P2X1 and P2X2 receptors and the P2X1 Cys2(1-6) chimera. n = 3-4 for all data sets and error bars indicate S.E.M. The inset shows the time-course of the ATP-evoked response to a maximum concentration of ATP. The different colours represent the WT P2X1 receptor (black), WT P2X2 receptor (red) and the P2X1 Cys2(1-6) chimera (blue). The black bar represents the 3 second application of ATP.

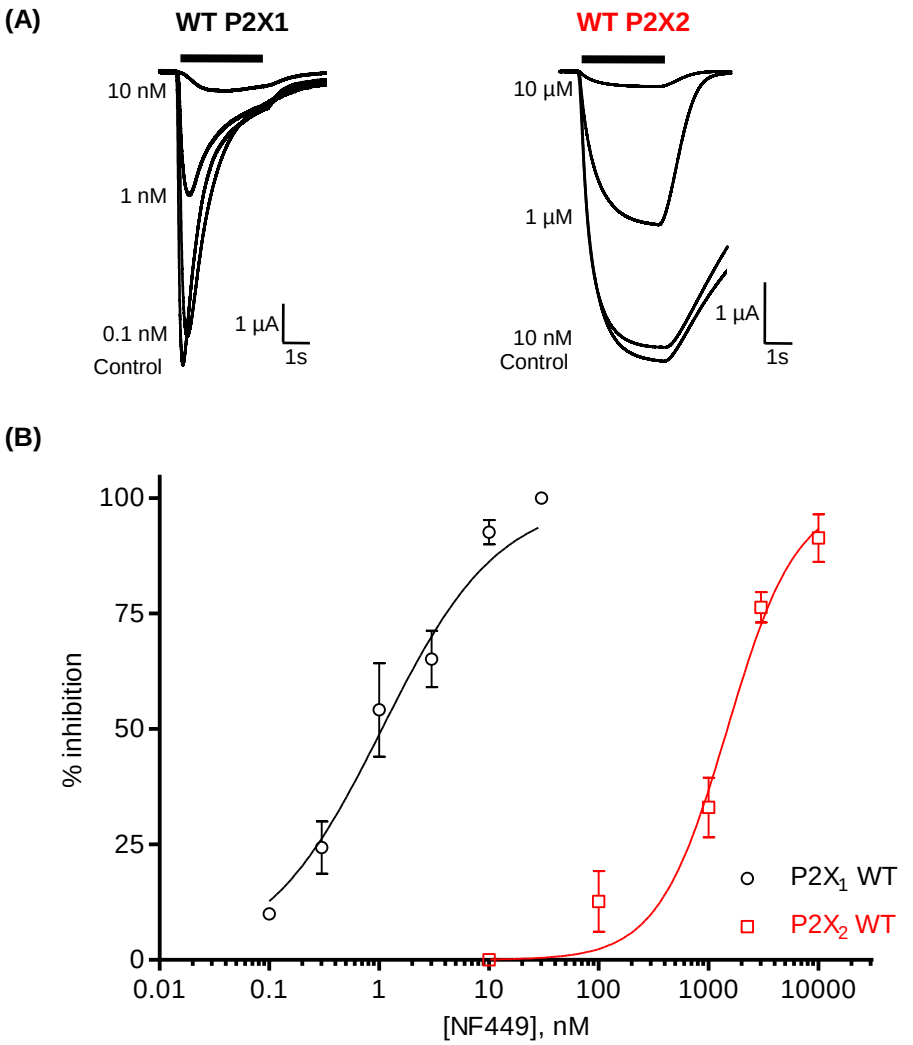

Figure 5.4. Characterisation of NF449 action at P2X1 and P2X2 receptors.
(A) Inhibition of ATP-evoked responses (EC_{90} concentration) by different concentrations of NF449 at the P2X1 and P2X2 receptors. NF449 was applied for 5 minutes before being co-applied with ATP for 3s (represented by black bar). **(B)** Concentration dependent inhibition curves of the wild type P2X1 (black) and P2X2 (red) receptors by NF449 to an EC_{90} concentration of ATP (n = 3-4 for all data sets). Error bars indicate S.E.M.

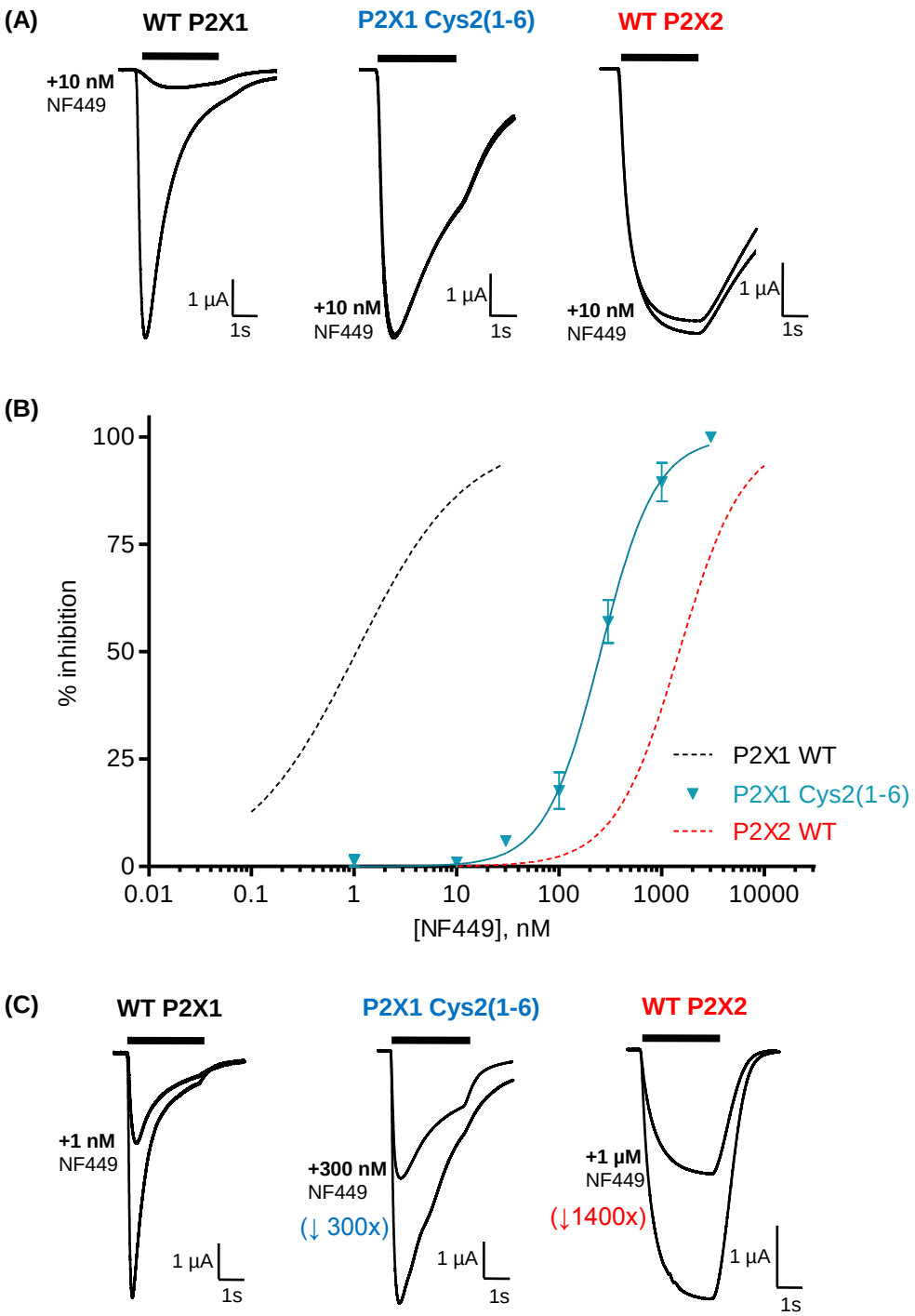

Figure 5.5. NF449 action at the P2X1 Cys2(1-6) chimera.
(A) Inhibition of ATP-evoked responses (EC_{90} concentration) by NF449 (10 nM) at the WT P2X receptors and the P2X1 Cys2(1-6) chimera. NF449 was for applied 5 minutes before being co-applied with ATP for 3s (indicated by black bar). **(B)** Concentration dependent inhibition curves of the P2X1 Cys2(1-6) chimera (cyan) by NF449 to an EC_{90} concentration of ATP. WT P2X1 and WT P2X2 are represented by black and red dotted lines, respectively. n = 3-4 for all data sets and error bars indicate S.E.M. **(C)** Inhibition of ATP-evoked currents (EC_{90} concentration of ATP) in the absence and presence of an ~IC_{50} concentration of NF449. The approximate fold change compared to the P2X1 receptor is shown in brackets. NF449 was for applied 5 minutes before being co-applied with ATP for 3s (indicated by black bar).

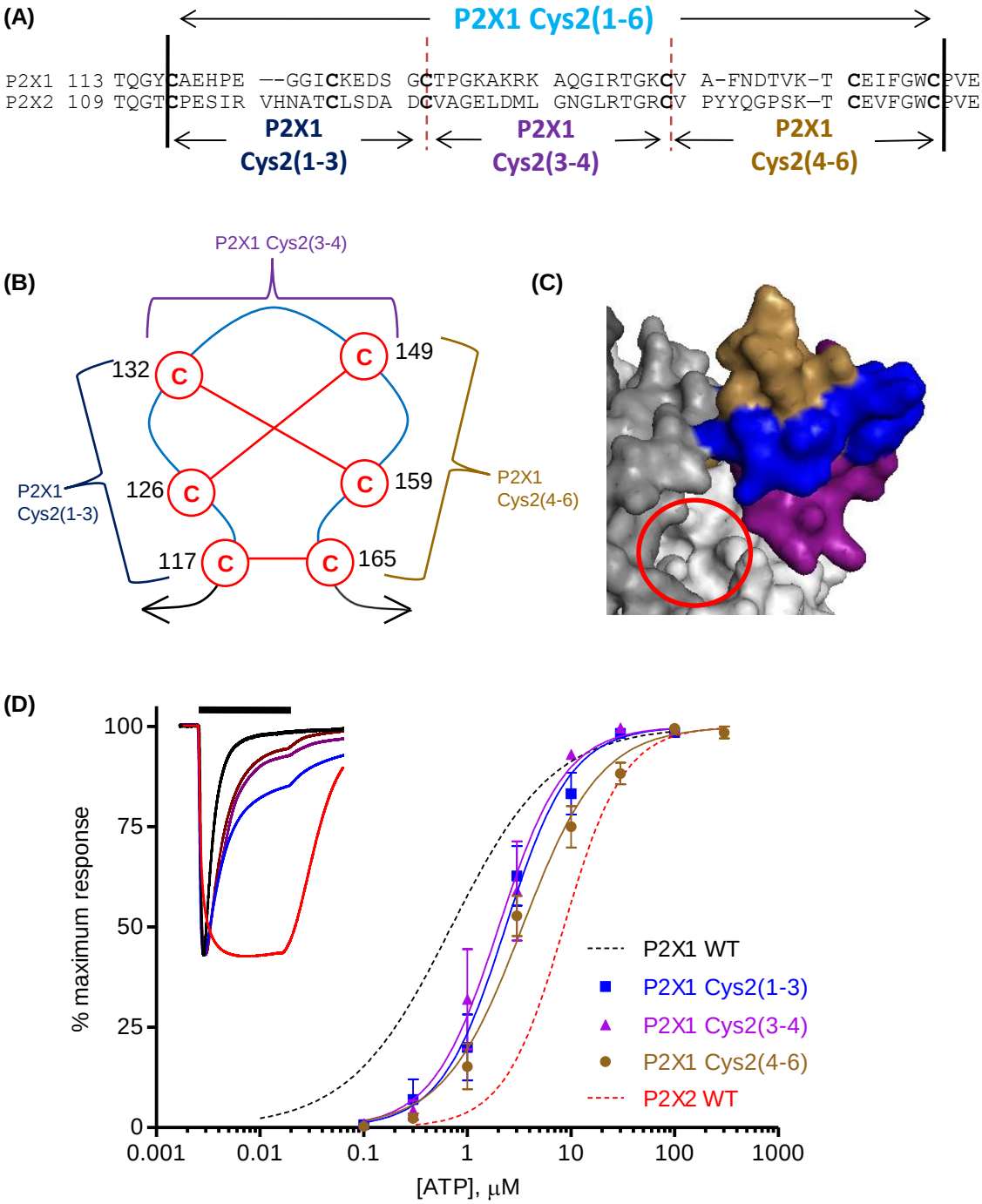

Figure 5.6. Characterisation of ATP action at the sub-divided chimeras in the cysteine rich head region.

(A) Sequence alignment of the P2X1 and P2X2 receptors showing the cross over points of the sub-divided chimeras. **(B)** Cartoon of the parings of the conserved cysteine residues where the chimeras were swapped at. **(C)** Surface rendering of the homology model of the P2X1 receptor with the different chimeras highlighted in blue (P2X1 Cys2(1-3)), purple (P2X1 Cys2(3-4)) and brown (P2X1 Cys2(4-6)). The predicted location of ATP is shown with a red circle. **(D)** Concentration-response curves to ATP of the different chimeras, with the wild type curves shown with dotted lines. n = 3-4 for all data sets and error bars indicate S.E.M. The inset shows the time-course of the ATP-evoked response to a maximum concentration of ATP with the 3 seconds application ATP shown by a black bar. The different colours represent the different chimeras and WT P2X receptors (colour coded as shown on the graph).

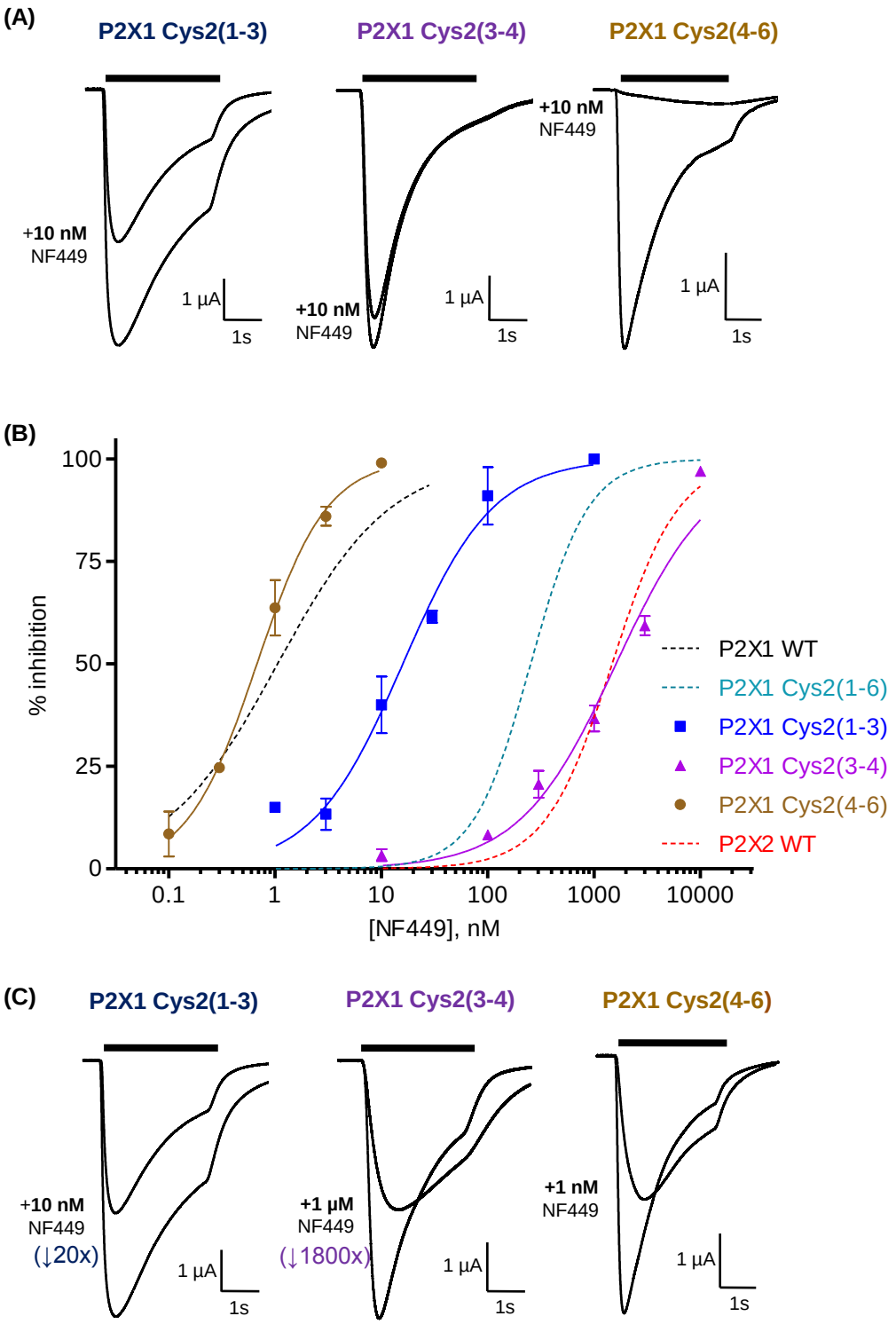

Figure 5.7. NF449 action at the sub-divided P2X1 chimeras

(A) Inhibition of ATP-evoked responses (EC_{90} concentration) by NF449 (10 nM) at the P2X1 Cys2(1-3), P2X1 Cys2(3-4) and P2X1 Cys2(4-6) chimeras. NF449 was applied for 5 minutes before being co-applied with ATP for 3s (indicated by black bar). **(B)** Concentration dependent inhibition curves of the individual chimeras by NF449 to an EC_{90} concentration of ATP. The WT P2X receptors and the P2X1 Cys2(1-6) chimera are shown with dotted lines. n = 3-4 for all data sets and error bars indicate S.E.M. **(C)** Inhibition of ATP-evoked currents (EC_{90} concentration of ATP) in the absence and presence of an ~IC_{50} concentration of NF449. The approximate fold change compared to the P2X1 receptor is shown in brackets. NF449 was for applied 5 minutes before being co-applied with ATP for 3s (indicated by black bar).

(A)

```
P2X1: 132  CTPGKAKRKA QGIRTGKC 149
P2X2: 130  CVAGELDMLG NGLRTGRC 147
```

(B) (i) **(ii)**

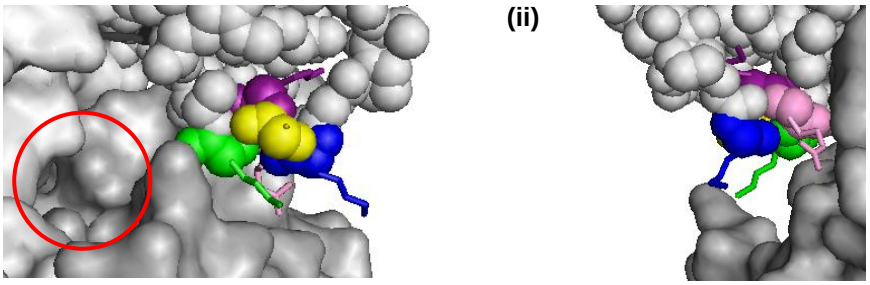

(C)

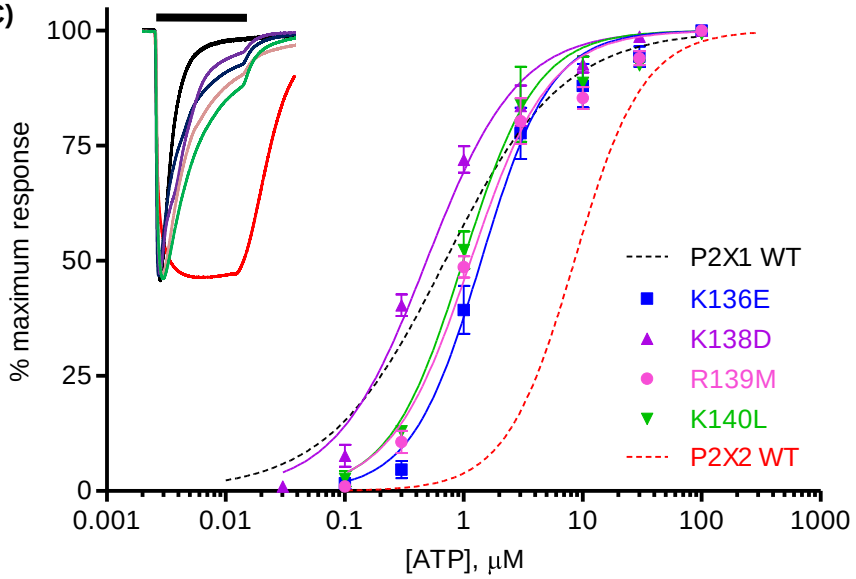

Figure 5.8. ATP action at the point mutants that remove an individual positively charged residue from the P2X1 receptor.

(A) Sequence alignment of the P2X1 and P2X2 receptors with the residues that were mutated in red. Conserved residues are shown in bold. **(B)** Homology model of the P2X1 receptor zoomed in on the base of the cysteine head region. The cysteine rich head region is shown in spheres with the residues K136-K140 having their main chain in spheres and side chain in sticks. (K136 in blue, A137 in yellow, K138 in purple, R139 in pink and K140 in green). The residues are shown in two views; **(i)** showing the ATP binding pocket and **(ii)** rotated to show the back of the cysteine rich head region head and the groove underneath. Predicted position of ATP is shown with a red circle. **(C)** Concentration-response curves to ATP on the different P2X1 receptor point mutants. Wild type responses are shown by dotted lines. The inset shows the time-course of the ATP-evoked response to a maximum concentration of ATP with the 3 second application of ATP shown by a black bar. The different colours represent the different WT and mutant P2X receptors (colour coded as shown on the graph). n = 3-4 for all data sets and error bars indicate S.E.M.

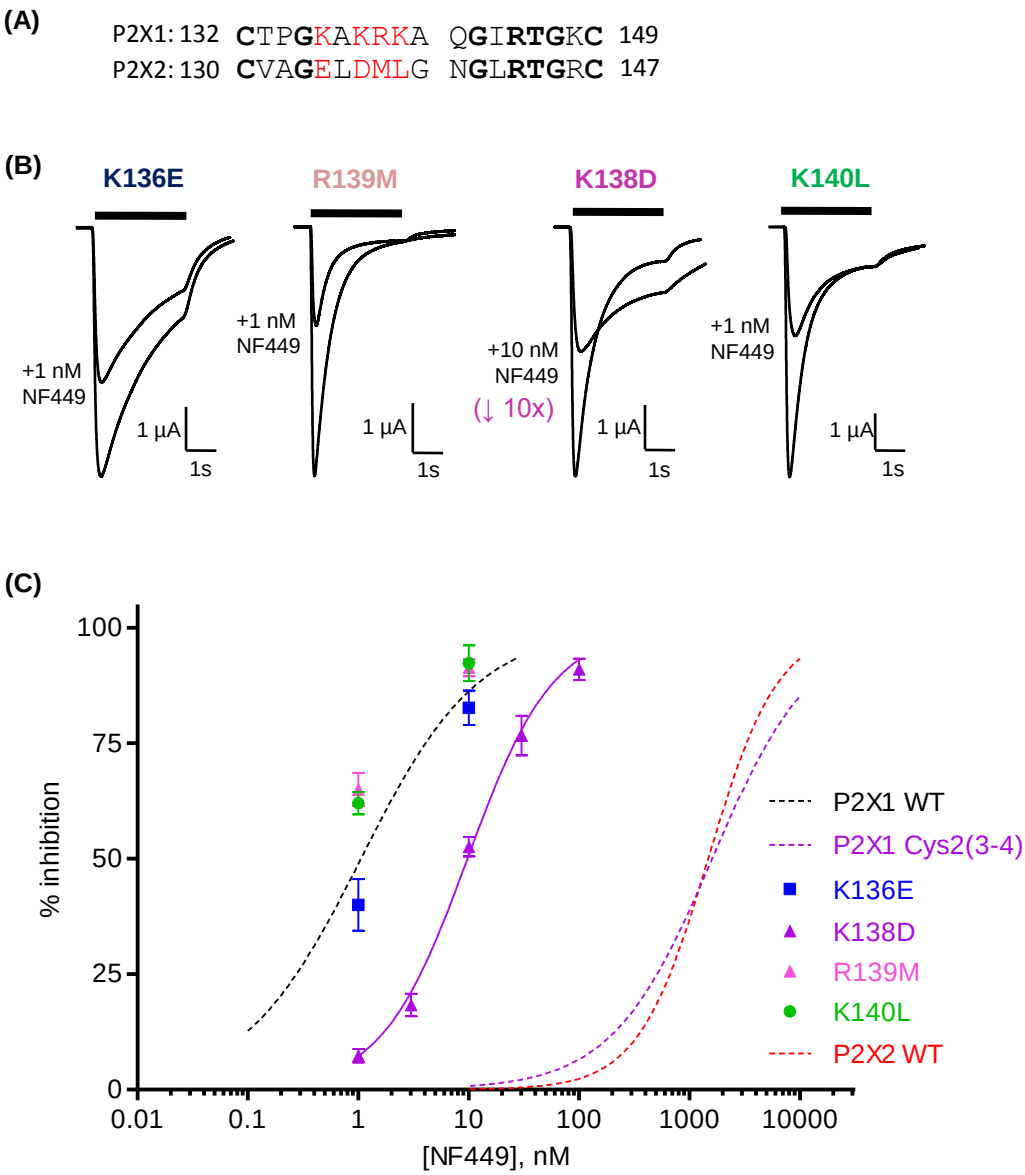

Figure 5.9. NF449 action at the single point mutants in the P2X1 receptor
(A) Sequence alignment of the P2X1 and P2X2 receptors with the residues that were mutated in red. Conserved residues are shown in bold. **(B)** Inhibition of ATP-evoked currents (EC_{90} concentration of ATP) in the absence and presence of an ~IC_{50} concentration of NF449. NF449 was applied for 5 minutes before being co-applied with ATP for 3s (indicated by black bar). The approximate fold change compared to the P2X1 receptor is shown in brackets. **(C)** Concentration dependent inhibition curves of the individual point mutants by NF449 to an EC_{90} concentration of ATP. The wild type receptors and the P2X1 Cys2(3-4) chimera are shown with dotted lines. n = 3-4 for all data sets and error bars indicate S.E.M.

(A)

P2X1: 132 **C**TP**G**KAKRKA QG**I**R**TG**K**C** 149
P2X2: 130 **C**VA**G**ELDMLG NG**L**R**TG**R**C** 147

(B)

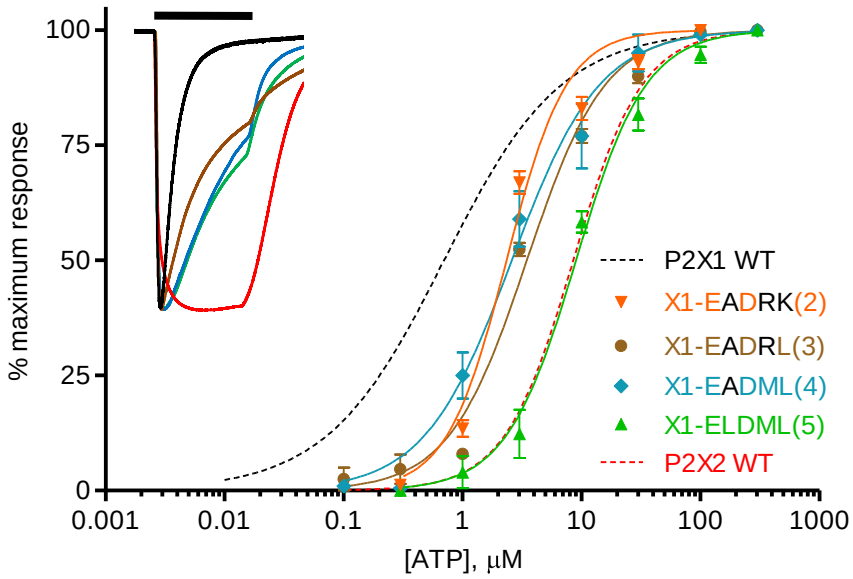

Figure 5.10. ATP action at the multiple point P2X1 receptor mutants.
(A) Sequence alignment of the P2X1 and P2X2 receptors with the residues that were mutated in red. Conserved residues are shown in bold. **(B)** Concentration-response curves to ATP at the multiple mutants in the P2X1 receptor. Dotted lines show the WT receptors. n = 3-4 for all data sets and error bars indicate S.E.M. The inset shows the time-course of the ATP-evoked response to the maximum concentration of ATP with the different colours representing the different WT and mutant receptors (colour coded as shown on the graph). The black line indicates the 3 second application of ATP.

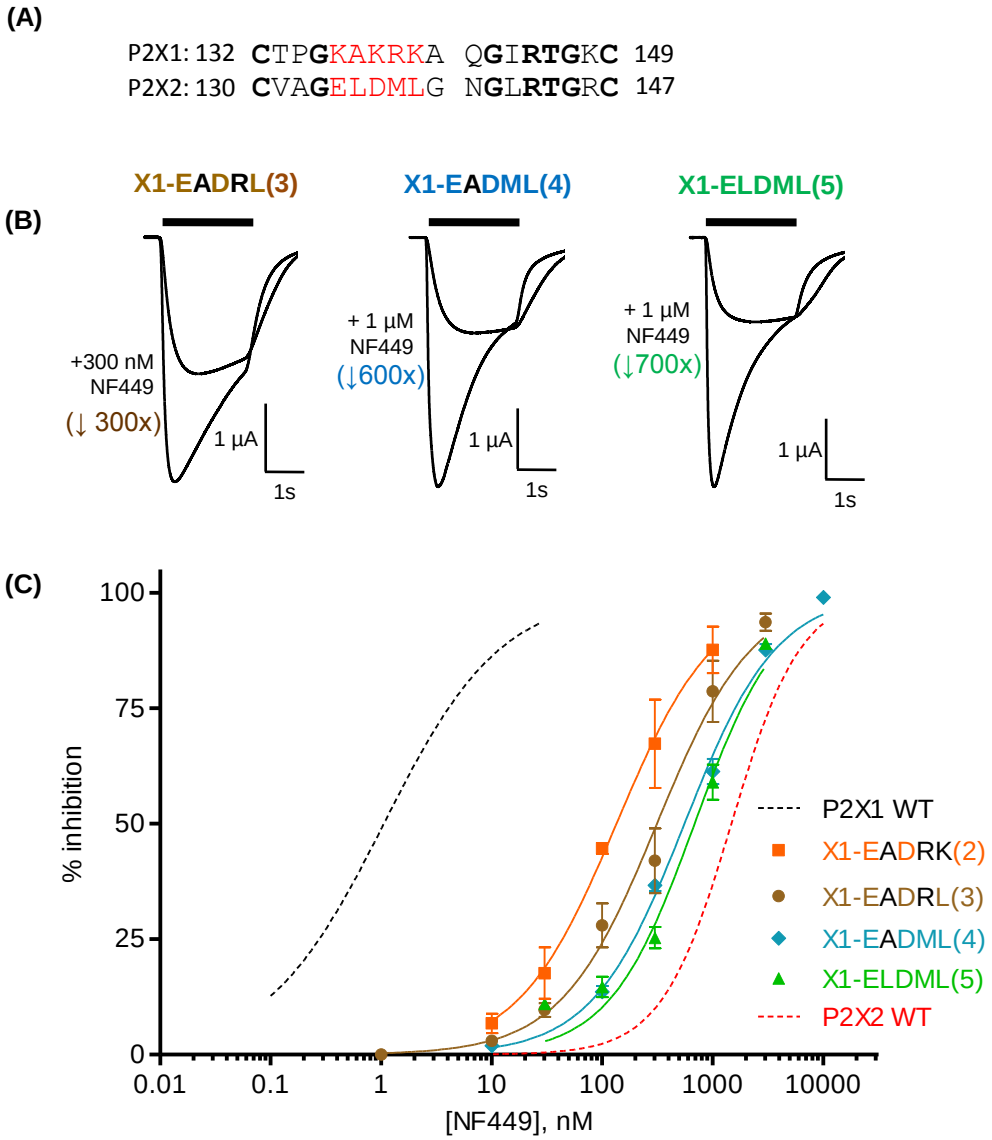

Figure 5.11. NF449 action at the multiple point P2X1 mutants.
(A) Sequence alignment of the P2X1 and P2X2 receptors with the residues that were mutated in red. Conserved residues are shown in bold. **(B)** Inhibition of ATP-evoked currents (EC_{90} concentration of ATP) in the absence and presence of an ~IC_{50} concentration of NF449. NF449 was applied for 5 minutes before being co-applied with ATP for 3s (indicated by black bar). The approximate fold change compared to the P2X1 receptor is shown in brackets. **(C)** Concentration dependent inhibition curves of the multiple point mutants by NF449 to an EC_{90} concentration of ATP. The WT receptors are shown with dotted lines. n = 3-4 for all data sets and error bars indicate S.E.M.

(A)

P2X1: 132 **C**TP**G**KAKRKA QG**I**R**TG**K**C** 149
P2X2: 130 **C**VA**G**ELDMLG N**G**L**RTG**R**C** 147

(B)

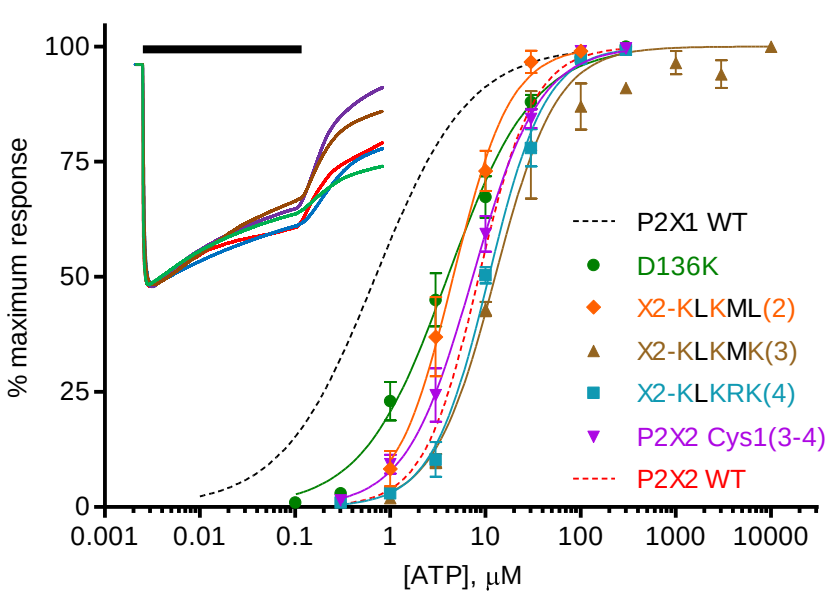

Figure 5.12. ATP action at the reciprocal mutant P2X2 receptors.
(A) Sequence alignment of the P2X1 and P2X2 receptors with the residues that were mutated in red. Conserved residues are shown in bold. **(B)** Concentration-response curves with ATP at the mutant P2X2 receptors and the P2X2 Cys1(3-4) chimera. Dotted lines show the WT receptors. The inset shows the time-course of the ATP-evoked response to the maximum concentration of ATP with the different colours representing the different WT and mutant receptors. The black line indicates the 15 second application of ATP.

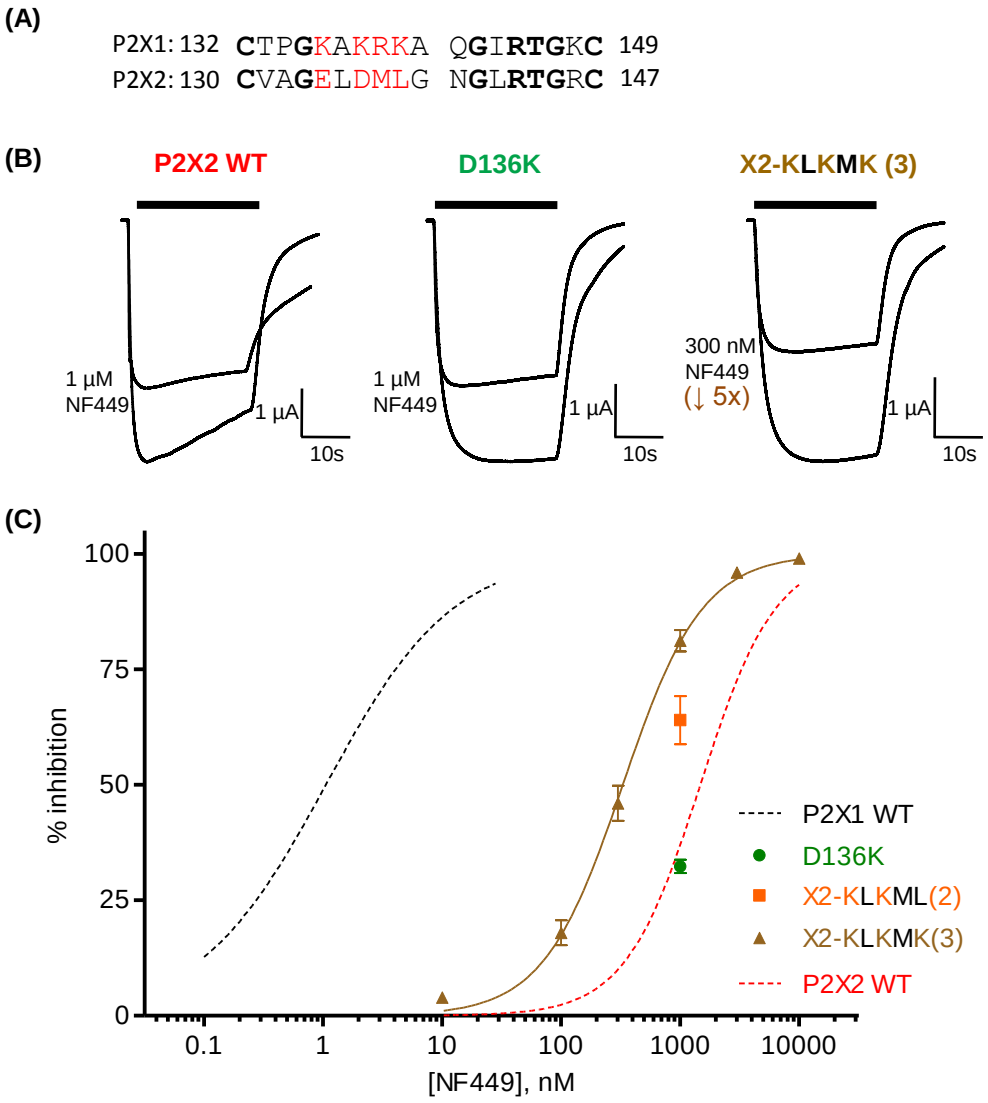

Figure 5.13. NF449 action at the reciprocal mutant P2X2 receptors.
(A) Sequence alignment of the P2X1 and P2X2 receptors with the residues that were mutated in red. Conserved residues are shown in bold. **(B)** Inhibition of ATP-evoked currents (EC_{90} concentration of ATP) in the absence and presence of an ~IC_{50} concentration of NF449. NF449 was applied for 5 minutes before being co-applied with ATP for 15s (represented by black bar). The approximate fold change compared to the P2X2 receptor is shown in brackets. **(C)** Concentration dependent inhibition curves of the P2X2 mutants by NF449 to an EC_{90} concentration of ATP. The WT receptors are shown with dotted lines. n = 3-4 for all data sets and error bars indicate S.E.M.

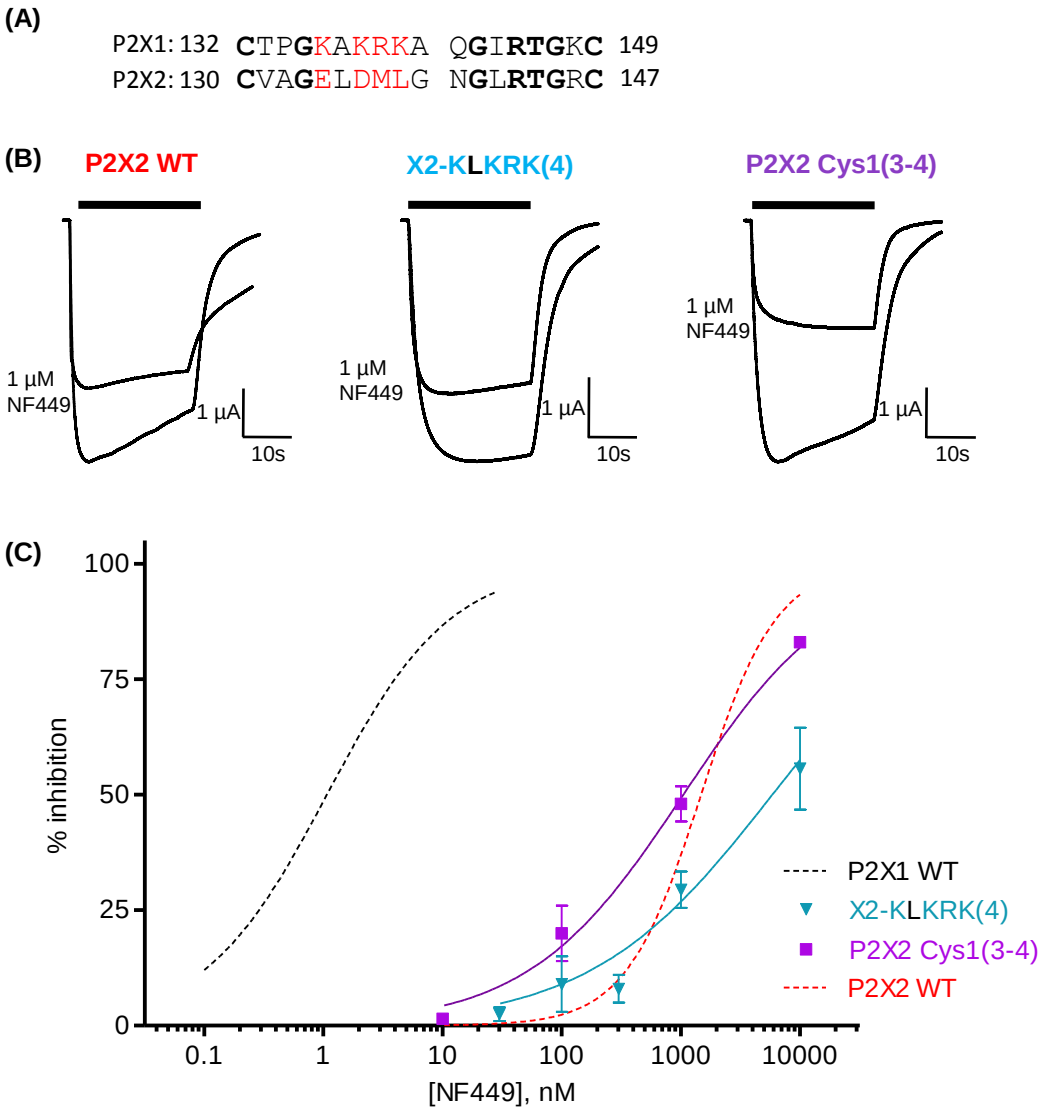

Figure 5.14. NF449 action at the reciprocal mutant P2X2 receptors.
(A) Sequence alignment of the P2X1 and P2X2 receptors with the residues that were mutated in red. Conserved residues are shown in bold. **(B)** Inhibition of ATP-evoked currents (EC_{90} concentration of ATP) in the absence and presence of an ~IC_{50} concentration of NF449. NF449 was applied for 5 minutes before being co-applied with ATP for 15s (represented by black bar). **(C)** Concentration dependent inhibition curves of the P2X2 mutants and P2X2 Cys1(3-4) chimera by NF449 to an EC_{90} concentration of ATP. The WT receptors are shown with dotted lines. n = 3-4 for all data sets and error bars indicate S.E.M.

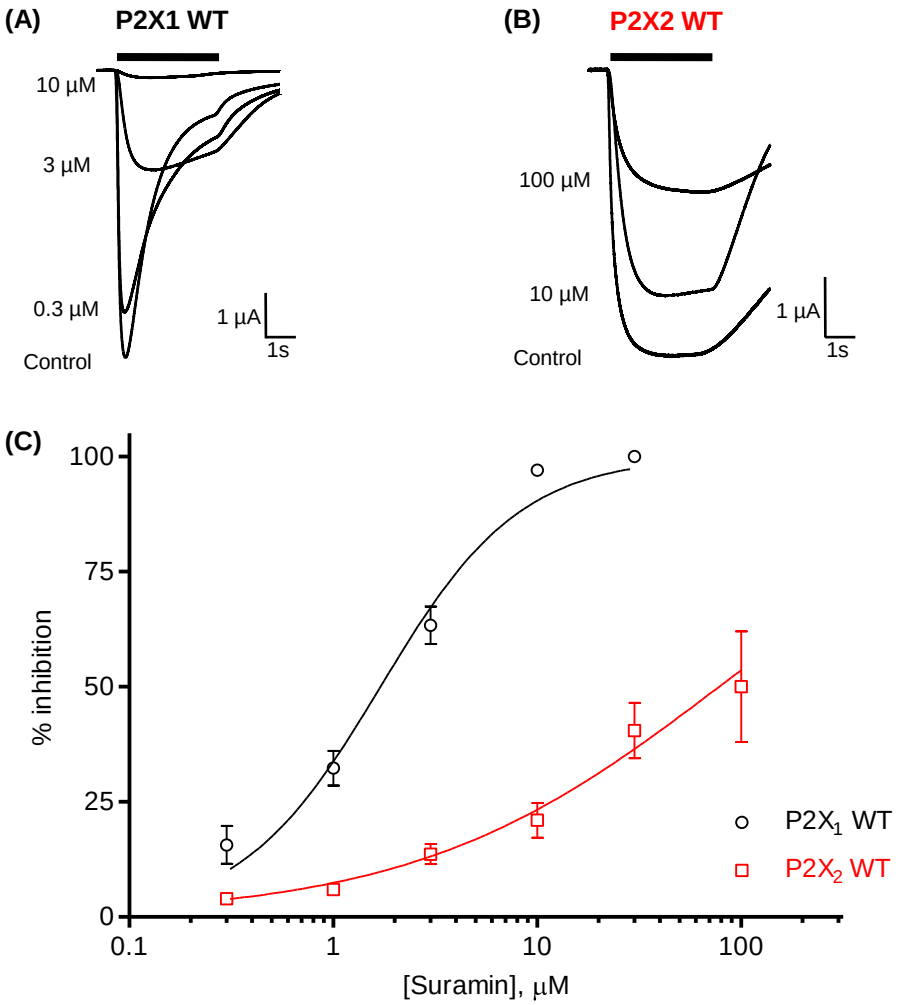

Figure 6.1. Characterisation of Suramin action at the P2X1 and P2X2 receptors.
(A) Inhibition of the ATP-evoked responses (EC_{90} concentration) by different concentrations of suramin at the P2X1 and P2X2 receptors. Suramin was applied for 5 minutes before being co-applied with ATP for 3s (represented by black bar). **(B)** Concentration dependent inhibition curves of the WT P2X1 (black) and P2X2 (red) receptors by suramin to an EC_{90} concentration of ATP. n = 3-4 for all data sets and error bars indicate S.E.M.

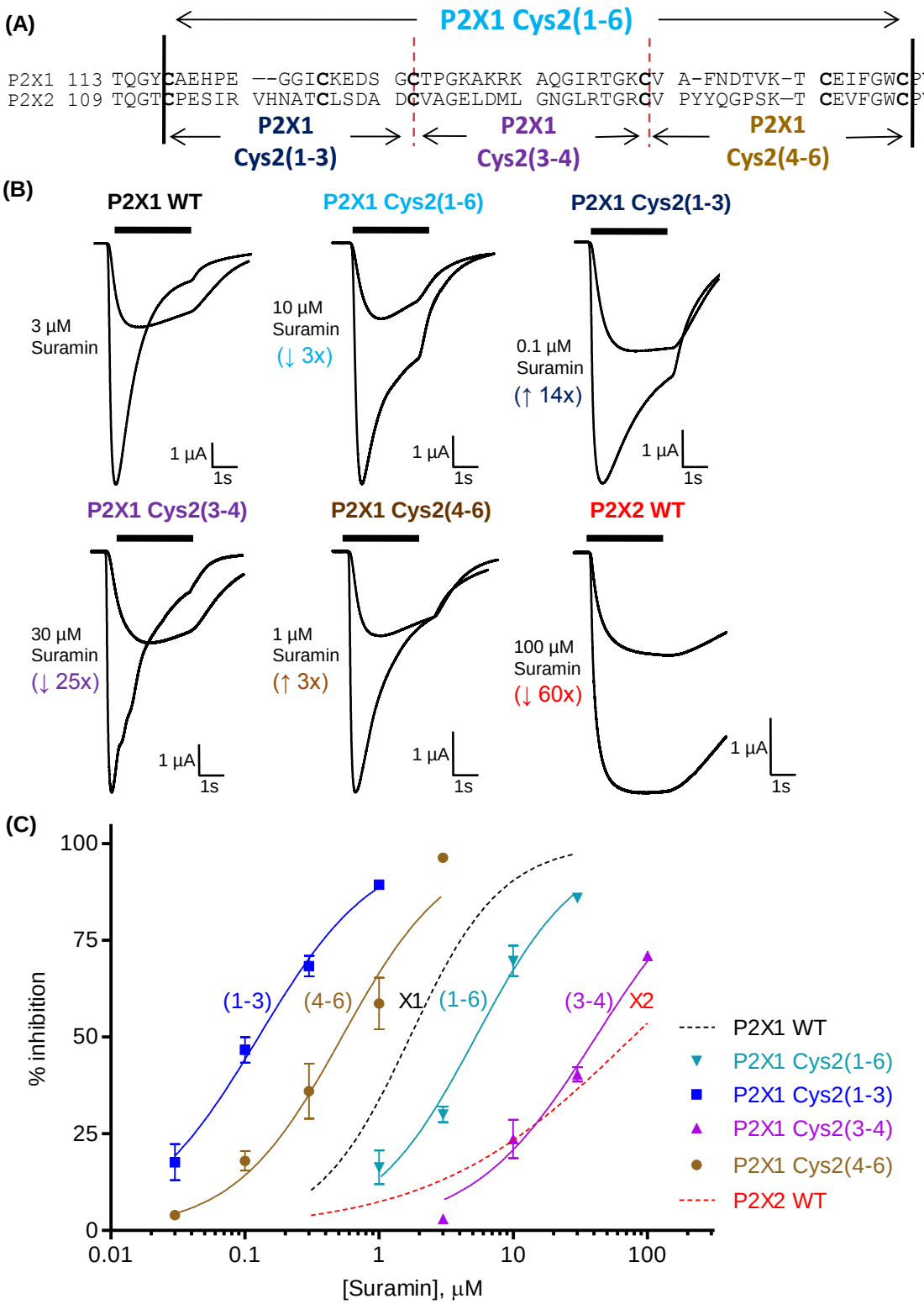

Figure 6.2. Suramin action at the P2X1 receptor chimeras.
(A) Sequence alignment of the P2X1 and P2X2 receptors showing the cross over points of the sub-divided chimeras. **(B)** Inhibition of ATP-evoked currents (EC_{90} concentration of ATP) in the absence and presence of an ~IC_{50} concentration of suramin. The approximate fold change compared to the P2X1 receptor is shown in brackets. Suramin was applied for 5 minutes before being co-applied with ATP for 3s (represented by black bar). **(C)** Concentration dependent inhibition curves of the individual chimeras by suramin to an EC_{90} concentration of ATP. The WT receptors are shown with dotted lines. n = 3-4 for all data sets and error bars indicate S.E.M.

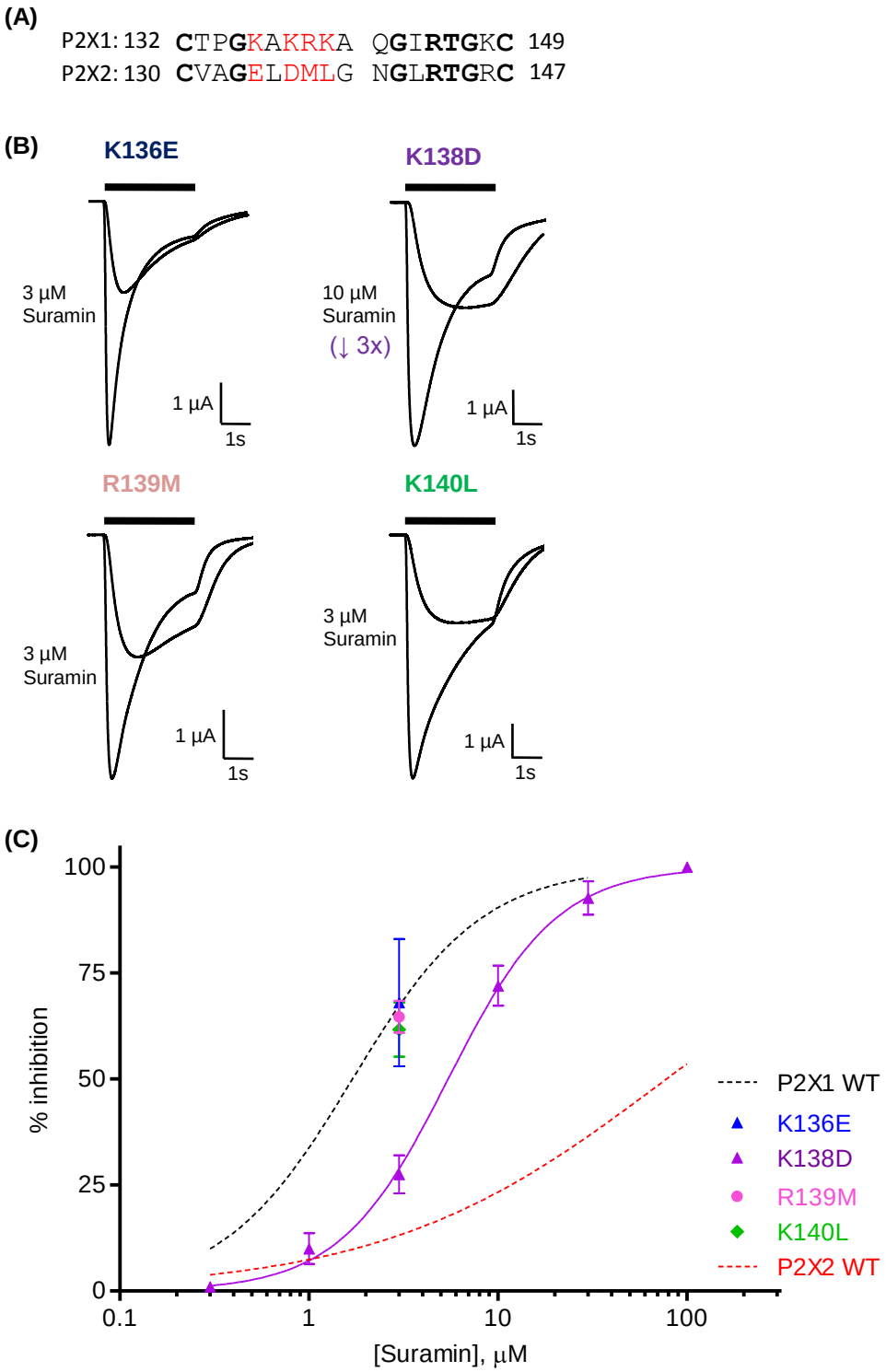

Figure 6.3 Suramin action at the single point mutants in the P2X1 receptor
(A) Sequence alignment of the P2X1 and P2X2 receptors with the residues that were mutated in red. Conserved residues are shown in bold. **(B)** Inhibition of ATP-evoked currents (EC_{90} concentration of ATP) in the absence and presence of an ~IC_{50} concentration of suramin. The approximate fold change compared to the P2X1 receptor is shown in brackets. Suramin was applied for 5 minutes before the application of ATP and then co-applied with ATP for 3s (represented by black bar). . **(C)** Concentration dependent inhibition curves of the individual point mutants by suramin to an EC_{90} concentration of ATP. The wild type receptors are shown with dotted lines. n = 3-4 for all data sets and error bars indicate S.E.M.

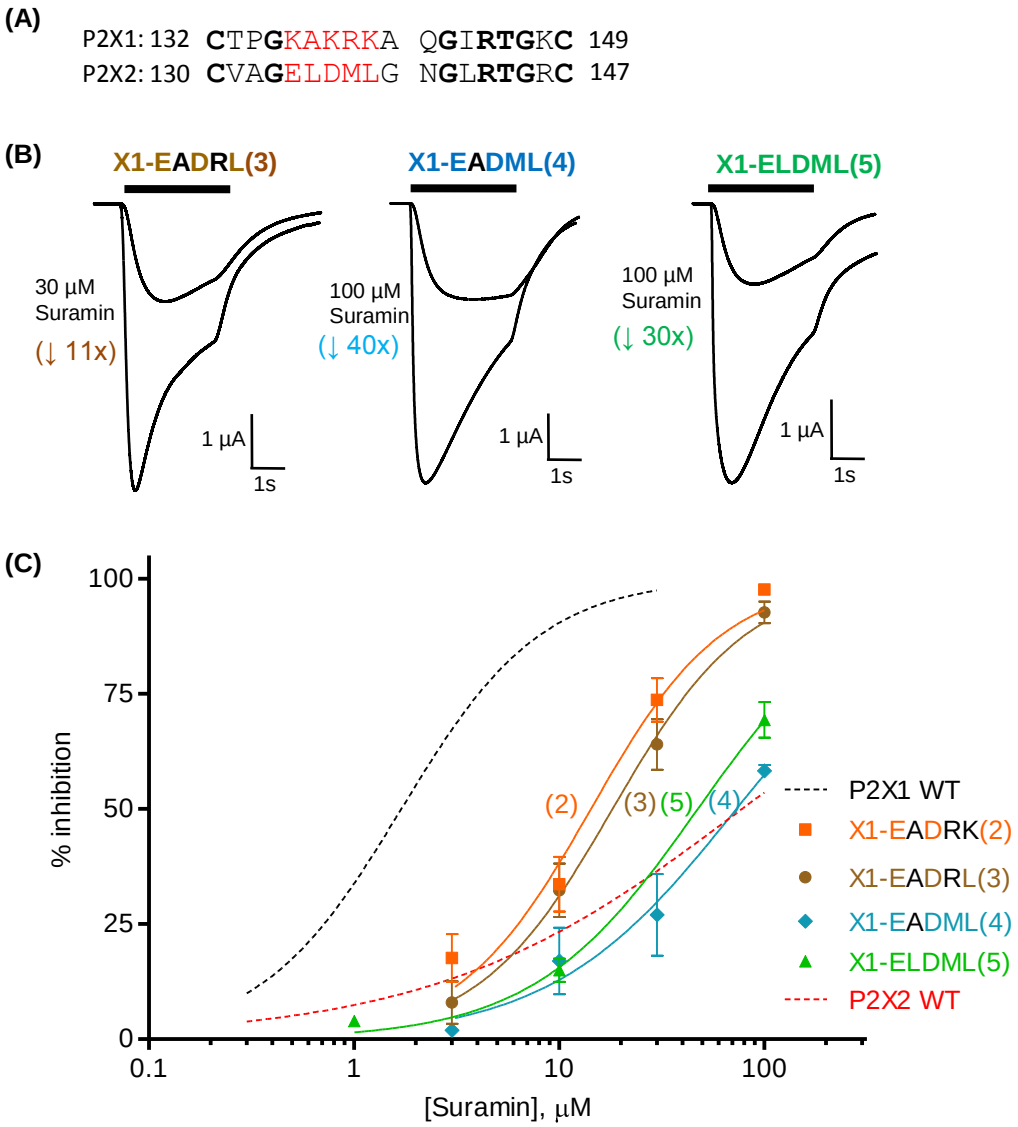

Figure 6.4 Suramin action at the multiple point P2X1 receptor mutants.
(A) Sequence alignment of the P2X1 and P2X2 receptors with the residues that were mutated in red. Conserved residues are shown in bold. **(B)** Inhibition of ATP-evoked currents (EC_{90} concentration of ATP) in the absence and presence of an ~IC_{50} concentration of suramin. The approximate fold change compared to the P2X1 receptor is shown in brackets. Suramin was applied for 5 minutes before being co-applied with ATP for 3s (represented by black bar). **(C)** Concentration dependent inhibition curves of the multiple point mutants by suramin to an EC_{90} concentration of ATP. The WT receptors are shown with dotted lines. n = 3-4 for all data sets and error bars indicate S.E.M.

(A)

P2X1: 132 **C**TP**G**KAKRKA QG**I**R**TG**K**C** 149
P2X2: 130 **C**VA**G**ELDMLG NG**L**R**TG**R**C** 147

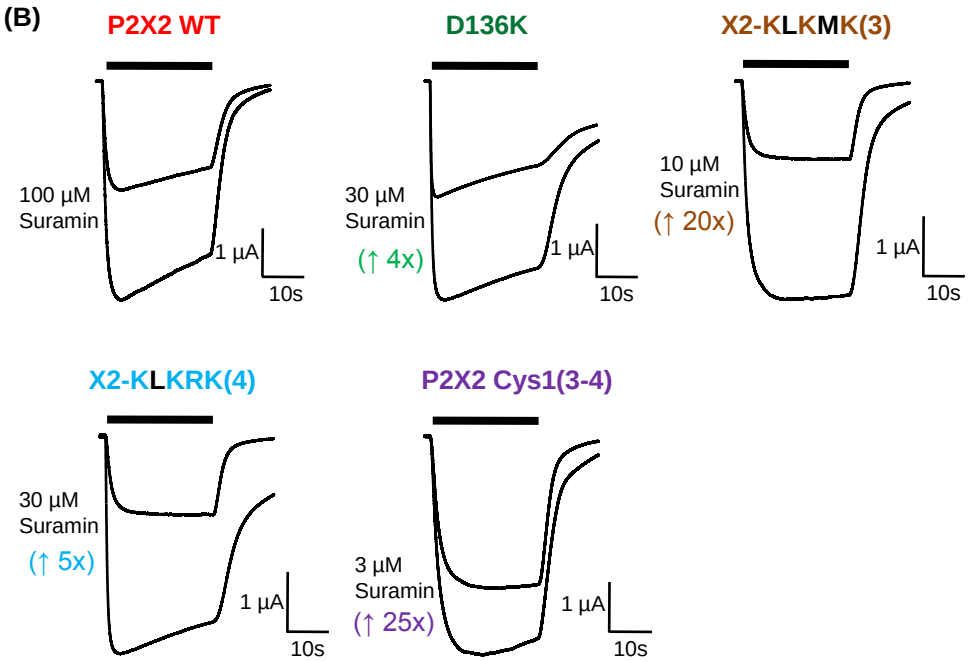

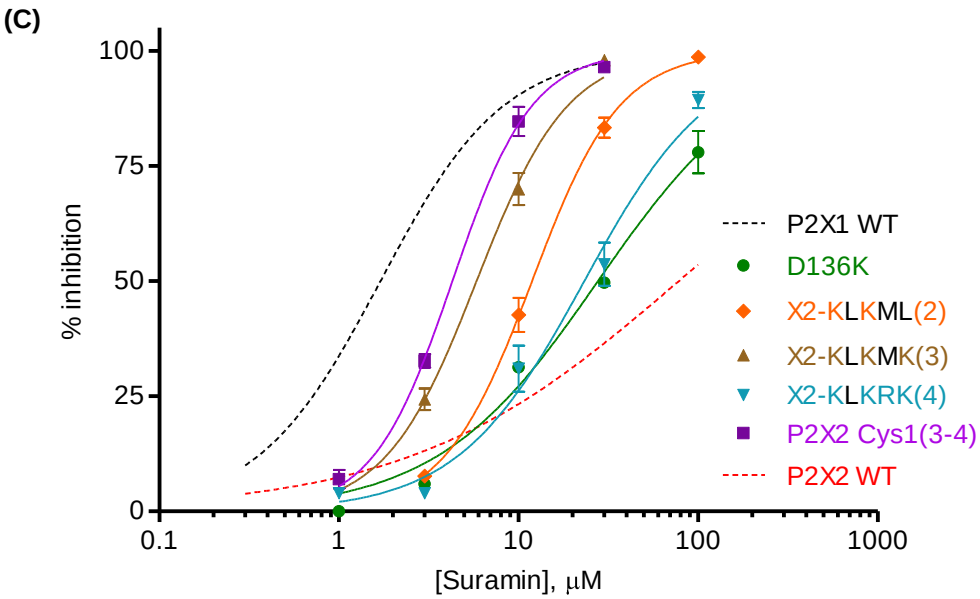

Figure 6.5. Suramin action at the reciprocal mutant P2X2 receptors.
(A) Sequence alignment of the P2X1 and P2X2 receptors with the residues that were mutated in red. Conserved residues are shown in bold. **(B)** Inhibition of ATP-evoked currents (EC_{90} concentration of ATP) in the absence and presence of an ~IC_{50} concentration of suramin. The approximate fold change compared to the P2X2 receptor is shown in brackets. Suramin was applied for 5 minutes before being co-applied with ATP for 15s (represented by black bar). **(C)** Concentration dependent inhibition curves of the P2X2 mutants by suramin to an EC_{90} concentration of ATP. The WT receptors are shown with dotted lines. n = 3-4 for all data sets and error bars indicate S.E.M.

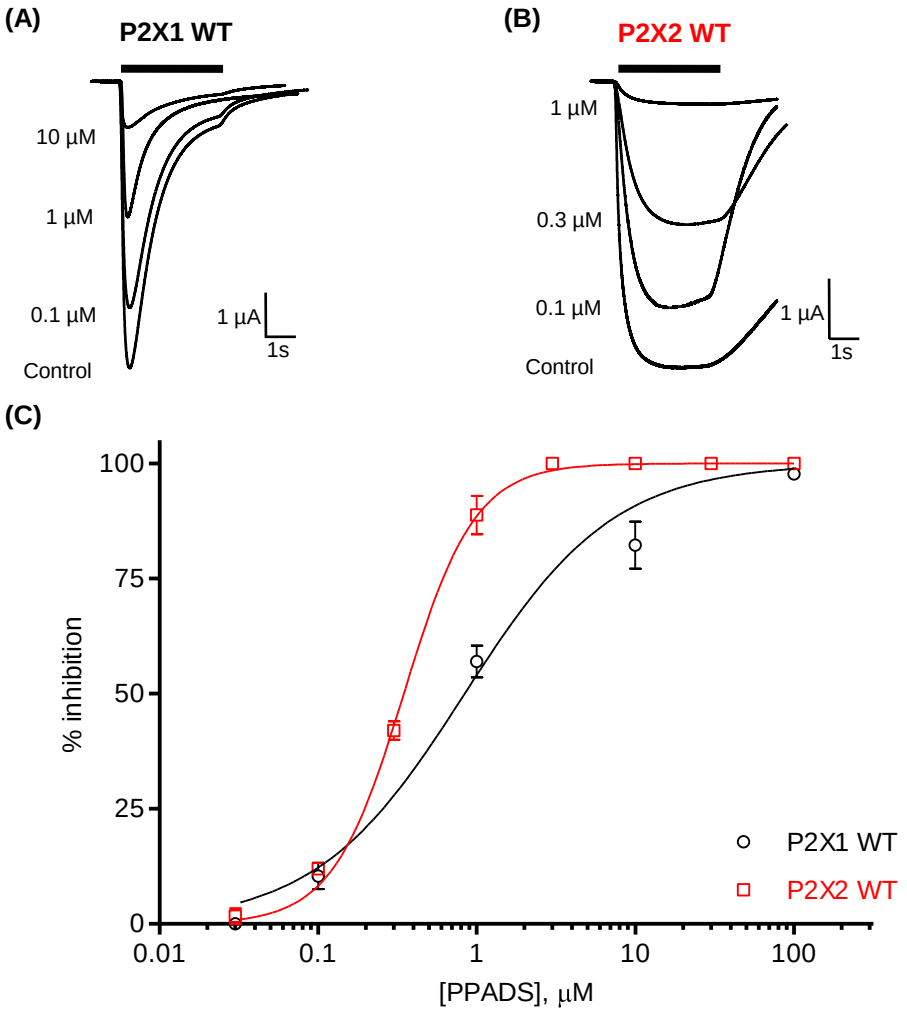

Figure 6.6. Characterisation of PPADS action at the P2X1 and P2X2 receptors.
(A) Inhibition of ATP-evoked responses (EC_{90} concentration) by different concentrations of PPADS at the P2X1 and P2X2 receptors. PPADS was applied for 5 minutes before being co-applied with ATP for 3s (represented by black bar). **(B)** Concentration dependent inhibition curves of the WT P2X1 (black) and P2X2 (red) receptors by PPADS to an EC_{90} concentration of ATP. n = 3-4 for all data sets and error bars indicate S.E.M.

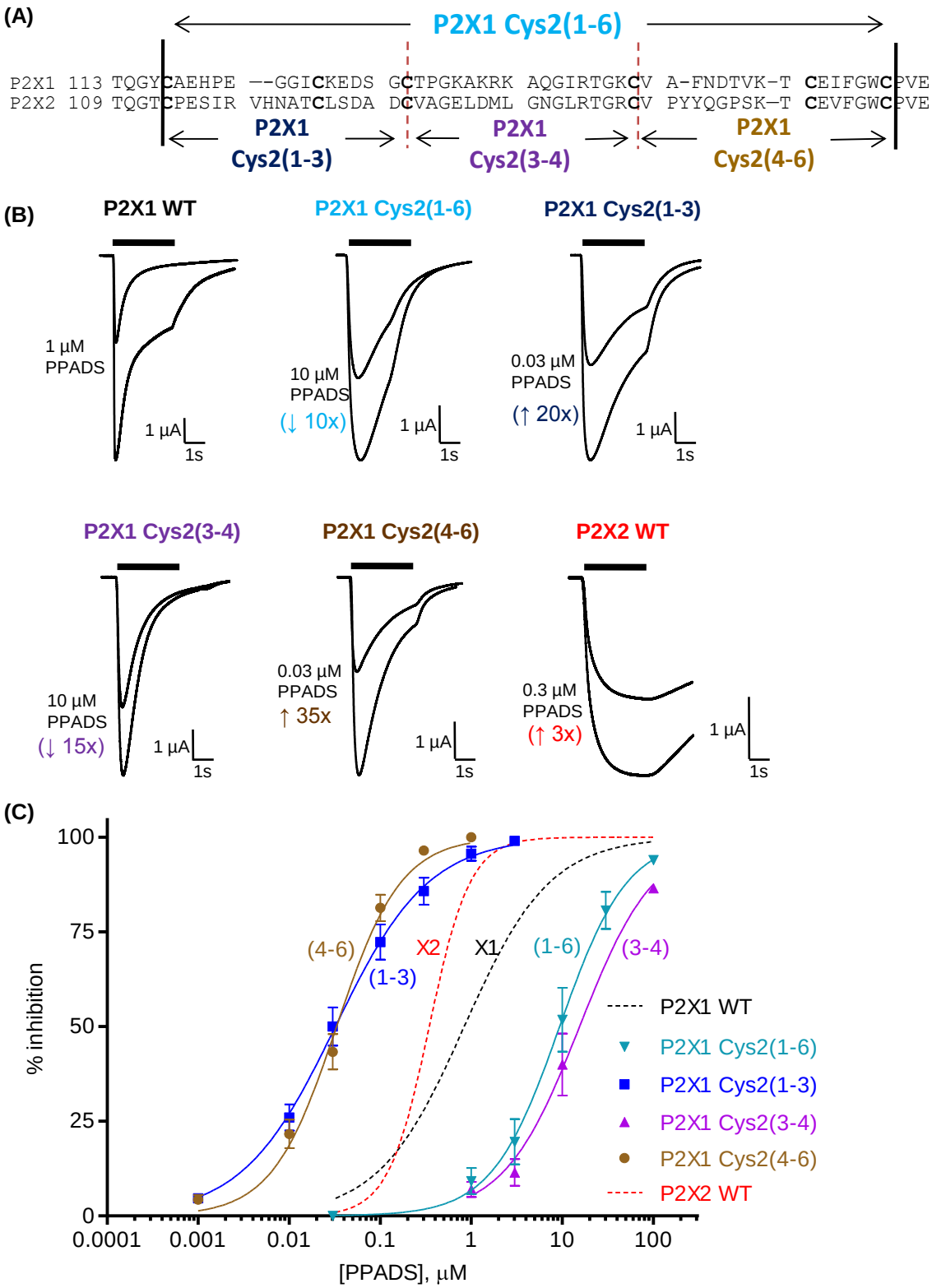

Figure 6.7. PPADS action at the P2X1 receptor chimeras.
(A) Sequence alignment of the P2X1 and P2X2 receptors showing the cross over points of the sub-divided chimeras. **(B)** Inhibition of ATP-evoked currents (EC_{90} concentration of ATP) in the absence and presence of an ~IC_{50} concentration of PPADS. The approximate fold change compared to the P2X1 receptor is shown in brackets. PPADS was applied for 5 minutes before being co-applied with ATP for 3s (represented by black bar). **(C)** Concentration dependent inhibition curves of the individual chimeras by PPADS to an EC_{90} concentration of ATP. The WT receptors are shown with dotted lines. n = 3-4 for all data sets and error bars indicate S.E.M.

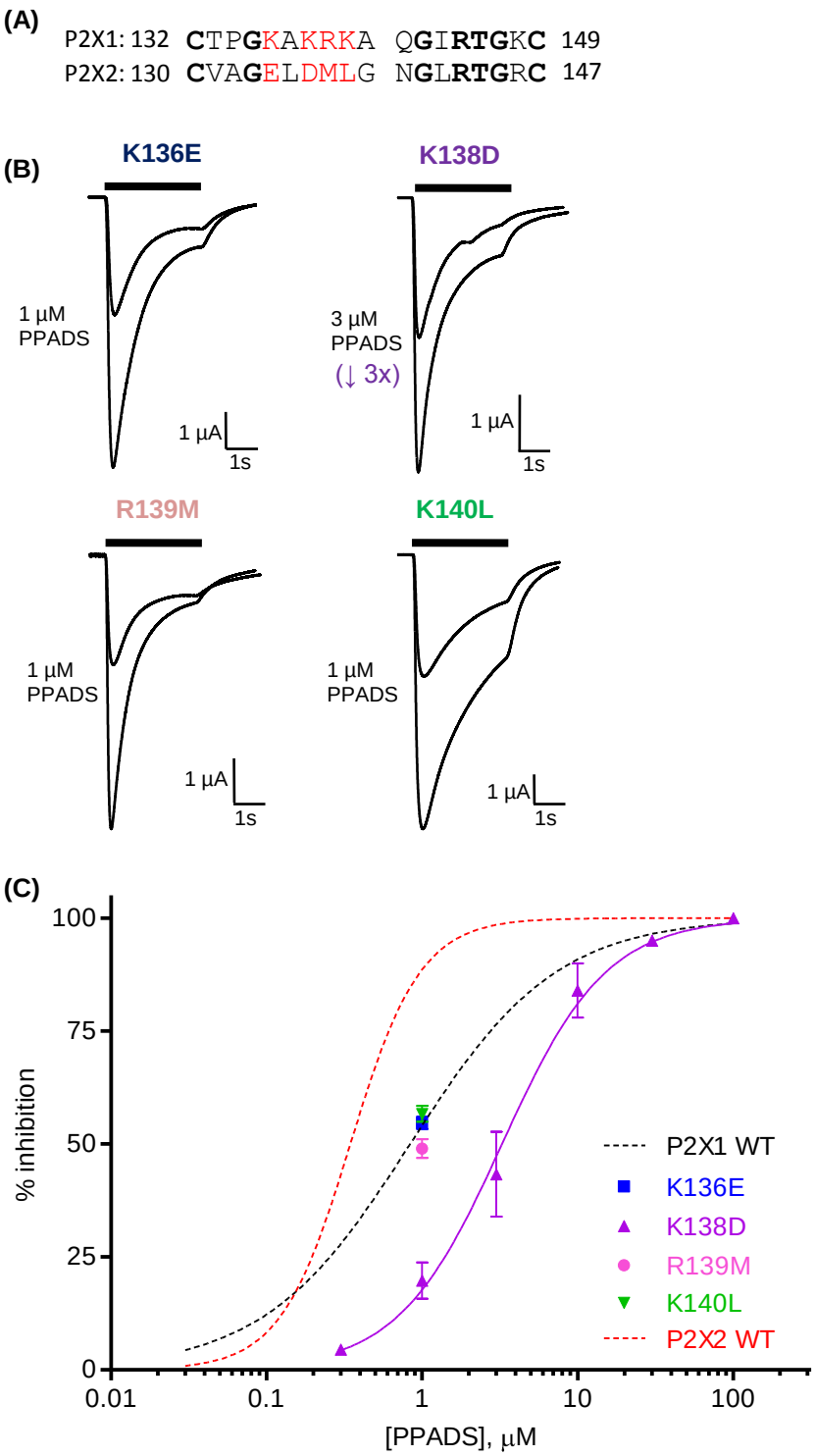

Figure 6.8. PPADS action at the single point mutants in the P2X1 receptor.
(A) Sequence alignment of the P2X1 and P2X2 receptors with the residues that were mutated in red. Conserved residues are shown in bold. **(B)** Inhibition of ATP-evoked currents (EC_{90} concentration of ATP) in the absence and presence of an ~IC_{50} concentration of PPADS. The approximate fold change compared to the P2X1 receptor is shown in brackets. PPADS was applied for 5 minutes before being co-applied with ATP for 3s (represented by black bar). **(C)** Concentration dependent inhibition curves of the individual point mutants by PPADS to an EC_{90} concentration of ATP. The wild type receptors are shown with dotted lines. n = 3-4 for all data sets and error bars indicate S.E.M.

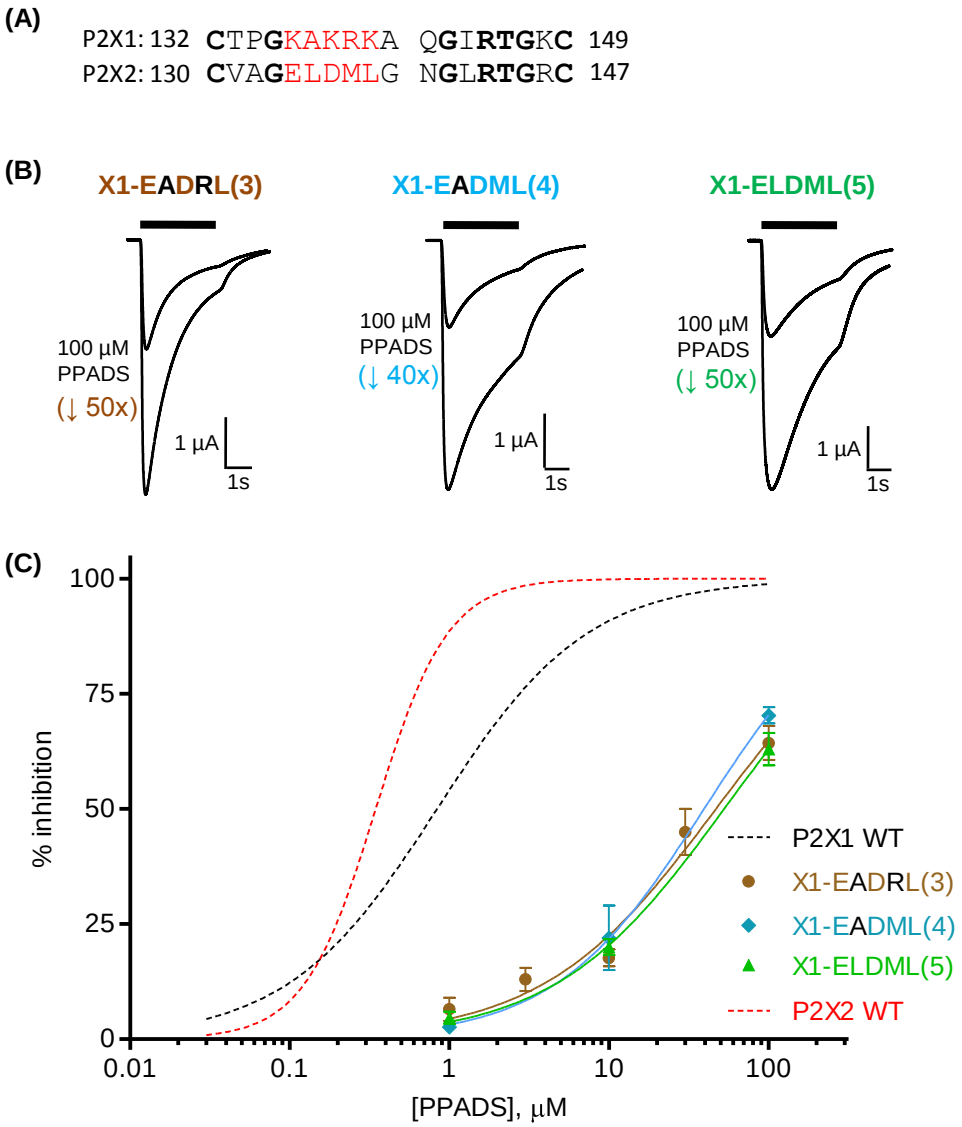

Figure 6.9. PPADS action at the multiple point P2X1 receptor mutants.
(A) Sequence alignment of the P2X1 and P2X2 receptors with the residues that were mutated in red. Conserved residues are shown in bold. **(B)** Inhibition of ATP-evoked currents (EC_{90} concentration of ATP) in the absence and presence of an ~IC_{50} concentration of PPADS. The approximate fold change compared to the P2X1 receptor is shown in brackets. PPADS was applied for 5 minutes before being co-applied with ATP for 3s (represented by black bar). **(C)** Concentration dependent inhibition curves of the multiple point mutants by PPADS to an EC_{90} concentration of ATP. The WT receptors are shown with dotted lines. n = 3-4 for all data sets and error bars indicate S.E.M.

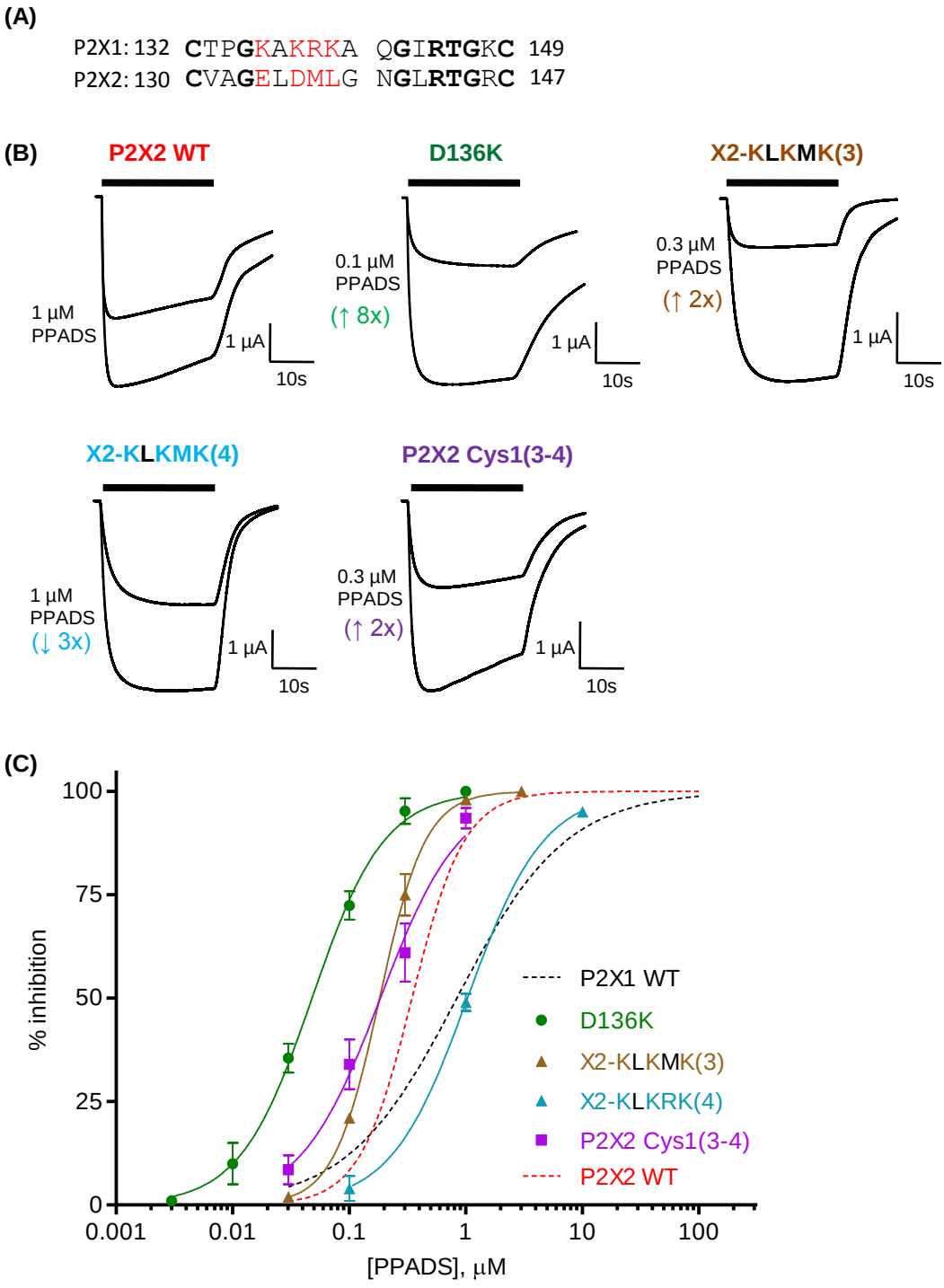

Figure 6.10. PPADS action at the reciprocal mutant P2X2 receptors.
(A) Sequence alignment of the P2X1 and P2X2 receptors with the residues that were mutated in red. Conserved residues are shown in bold. **(B)** Inhibition of ATP-evoked currents (EC_{90} concentration of ATP) in the absence and presence of an ~IC_{50} concentration of PPADS. The approximate fold change compared to the P2X2 receptor is shown in brackets. PPADS was applied for 5 minutes being co-applied with ATP for 15s (represented by black bar). **(C)** Concentration dependent inhibition curves of the P2X2 mutants by PPADS to an EC_{90} concentration of ATP. The WT receptors are shown with dotted lines. n = 3-4 for all data sets and error bars indicate S.E.M.